The Institute of Space and Astronautical Science
Report No. 644, March 1992

InP Solar Cells and their Flight Experiments

By

Keiji TAKAHASHI,* Masafumi YAMAGUCHI,[1] Tatsuya TAKAMOTO,[2] Shingo IKEGAMI,[3] Akira OHNISHI,* Tomonao HAYASHI,[4] Akio USHIROKAWA,[5] Masahiko KOHBATA,* Hidetoshi ARAI,[3] Katsumasa HASHIMOTO,[3] Takeshi ORII,[3] Hitoshi OKAZAKI,[2] Hideto TAKAMURA,[2] Mitsuru URA,[2] and Masamichi OHMORI[2]

Summary: We have developed high-efficiency homojunction 1 cm × 2 cm InP space solar cells by diffusing In_2S_3 into p type InP substrates and investigated their fundamental characteristics such as electrical and mechnical characteristics and thermal properties. On the radiation resistant mechanism of InP cells, we have studied InP cells fabricated at NTT Laboratories and found superior properties such as room temperture annealing and minority carrier injection enhanced annealing phenomena for radiation-induced defects in InP crystals with 1 MeV electron irradiation. We have also found that InP cells are superior to Si and GaAs cells in radiation resistance owing to the energy band structure and lower defect introduction rates of InP cells. Various tests were conducted to evaluate the developed InP cells in simulated space environments and to give them the qualification for space applications. In irradiation tests, proton energy was varied from 0.015 to 15 MeV with a fluence ranging from 10^{11} to 10^{13} protons/cm^2 and electron energy was varied from 0.5 to 3 MeV with a fluence ranging from 10^{14} to 10^{16} electrons/cm^2. As a result, we have confirmed that series resistance in the InP cells increases owing to a decrease in the majority carrier concentration at higher fluences even for proton irradiation. The developed InP cells were mounted on the twelfth scientific satellite "EXOS-D" as a radiation degradation characteristic instrument. The cells were also mounted on a lunar orbiter on board the thirteenth scientific satellite "MUSES-A" as a power source for the orbiter. We succeeded in working those InP cells in orbit. Large decreases in the short circuit current and in the open circuit voltage for the InP cells without coverglass on board the twelfth satellite turned out to be due to lower energy proton irradiation with our new analytical model. However, it has been confirmed that no degradation of the InP cells occurs by using thin coverglass of 50 μm in thickness. In the lunar orbiter, output power of its solar array was constant as predicted till the separation from the thirteenth satellite to place the orbiter in orbit around the moon. We have concluded that the InP solar cells are applicable to space solar cells under severe radiation environments in orbit.

Key words: high-efficiency solar cell, InP solar cell, environmental test, radiation resistance, scientific satellite.

* The Institute of Space and Astronautical Science
1 NTT Opto-electronics Laboratories
2 Electronic Materials & Components Research Laboratories, Nippon Mining Co., Ltd.
3 NEC Corporation
4 Chiba Institute of Technology
5 Tokyo Engineering University

1. Introduction

So far, Si solar cells have been used as a primary power source for space applications. However, recently power consumed by bus subsystems and scientific instruments for scientific satellites has been increasing remarkably because they have become larger and required more power for sophisticated and fine attitude and orbit control and scientific observations. In order to satisfy the requirement of the increase in consumed power, large structured solar cell arrays must be installed in the satellites. This tendency is disadvantageous to the satellite system weight since the payload capability of launch vehicles is limited. Under these circumstances light-weight, high-efficiency solar cells, i.e., cells with a large power to mass ratio are required. Thus, we, first of all, have developed high efficiency InP space solar cells.

Yamaguchi et al. [*1*] have recently fabricated InP solar cells at their laboratory, demonstrating 18 % conversion efficiency under the Air Mass 0 (AM0) condition. Solar cells for space applications, however, must also be resistant to space radiation such as charged particles (electrons and protons) in the Van Allen belt. They [*2, 3*] have reported that InP solar cells are superior to Si and GaAs cells in radiation resistance. They have also observed room temperature recovery phenomena of radiation damages in InP cells [*4*] and annealing phenomena for radiation-induced defects in InP cells due to minority carrier injection under light illumination and forward bias application [*5*]. Such superior radiation resistance of InP cells suggests that they are promising for space applications.

In order to realize InP space solar cells, it is necessary to conduct and evaluate proton and electron irradiation tests of the developed InP solar cells in wide energy range on the ground [*6, 7*]. The cells were irradiated with 0.015–15 MeV protons with a fluence ranging from 10^{11} to 10^{13} protons/cm^2, and with 0.5–3 MeV electrons with a fluence ranging from 10^{14} to 10^{16} electrons/cm^2. As a result, we have confirmed that series resistance in the InP cells increases owing to a decrease in the majority carrier concentration at higher fluences even with proton irradiation. We have also carried out their various environmental tests.

On the basis of these results we succeeded in launching two scientific satellites with the InP cells equipped with an instrument for monitoring their radiation degradation characteristics and with a lunar orbiter using the cells as a power source.

From flight data obtained with the instrument on board the twelfth scientific satellite, large decreases in the short circuit current and in the open circuit voltage for the cells without coverglass were observed. An analysis with our new model showed that the degradation is due to lower energy proton irradiation. However, we have confirmed that the use of thin coverglass of 50 μm in thickness prevents the degradation of the InP cells

In the lunar orbiter, output power of its solar array was constant as predicted till the separation from the thirteenth scientific satellite to place the orbiter in orbit around the moon.

Payload savings resulting from the radiation resistance of InP solar cells are especially favorable for large spacecraft. Weinberg et al. [*8*] have recently proposed

the adoption of an InP solar array with power generation capability of 12.2 kW at 5 years for a polar-orbiting platform, EOS (Earth Observing System) to be launched in late 1997 to study the Earth's environment and to advance the knowledge of both natural and human-induced global change. As can be seen with such an example, it seems that InP cells will be used more frequently for large spacecraft power systems in the future.

In this paper, we will mainly describe fabrication, fundamental characteristics, proton and electron irradiation tests, various environmental tests, and flight experiments of the developed InP solar cells.

2. Cell Fabrication

We have developed high-efficiency homojunction indium phosphide solar cells by closed-ampoule diffusion of In_2S_3 into p type substrates. Since InP solar cells have lower surface recombination velocity than that of GaAs solar cells, high efficiency can be expected with simple structure without a window layer. A large-scale, commercial process to produce InP solar cells has been developed.

Figure 1 shows the processing steps of our InP solar cell fabrication. The cell structure is shown in Fig. 2. More than one thousand three hundred 1 cm × 2 cm cells

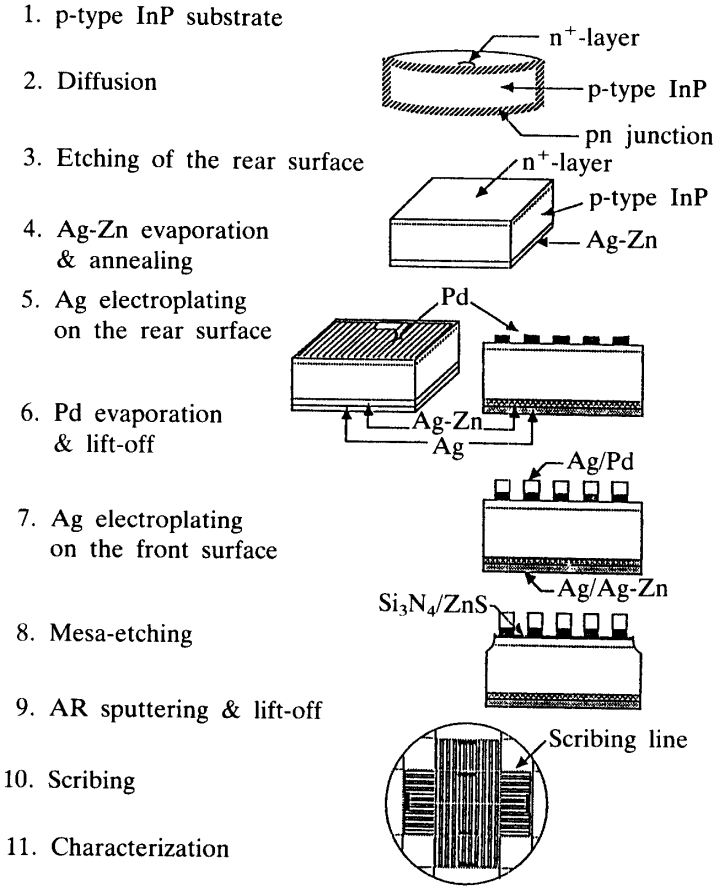

Fig. 1. Processing steps to fabricate n^+-p homojunction InP solar cells.

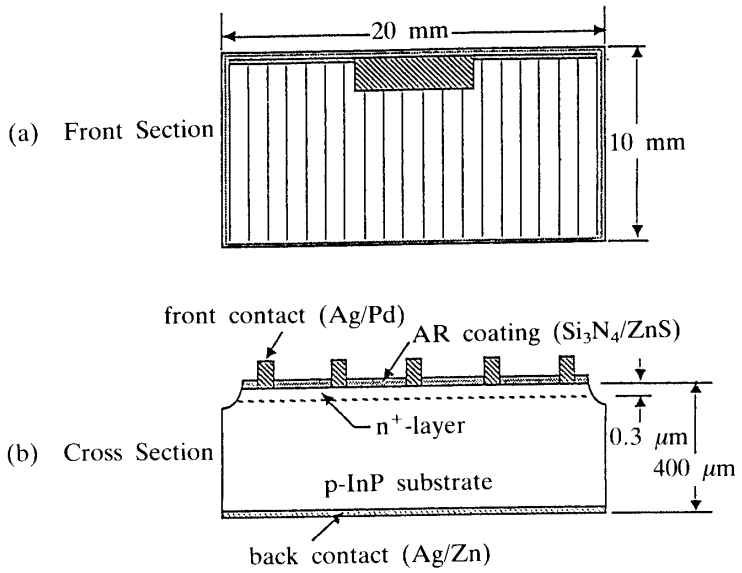

Fig. 2. Cell structure.

for the lunar orbiter were produced with the same process. The summary of the cell fabrication is described below.

2.1 Diffusion

The n^+-p homojunction of the InP solar cells was formed by diffusing sulphur into p type substrates which were grown in-house by liquid encapsulated Czochralski (LEC) method and supplied as two-inch polished wafers. The wafers were 400 μm thick, (100)-oriented, and doped with Zn to a carrier concentration of 2–5 × 10^{16} cm^{-3} as-grown; it should be noted that the carrier concentration measured after diffusion was 5–8 × 10^{16} cm^{-3} [9]. The diffusion was carried out in a sealed quartz ampoule (~1.2 liter in volume) as shown in Fig. 3 at 675 °C for 3 hours. In_2S_3 (4.5 g) was used as a diffusion source, and red phosphorus (0.4 g) was added to prevent thermal decomposition at the diffusion temperature. The surface carrier concentration was approximately 7–8 × 10^{18} cm^{-3} and the formed junction depth, x_j was about 0.3 μm. In one diffusion cycle, three hundred 1 cm × 2 cm cells were fabricated from 50 two-inch wafers.

A series of experiments were carried out to investigate the dependence of solar cell parameters on diffusion temperature, Td. The diffusion was conducted for 3 hours at

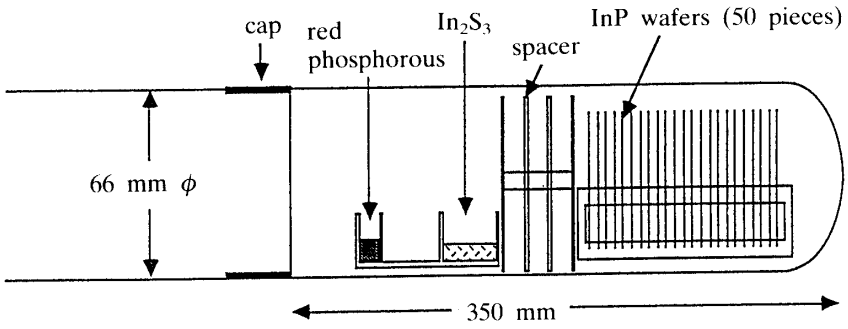

Fig. 3. An apparatus for diffusion process.

a temperature from 600 to 720 °C. The substrate carrier concentration before diffusion was 1–2 × 10^{16} cm^{-3}. Figure 4 shows the SIMS (Secondary Ion Mass Spectrometer) profiles of sulphur in the cells diffused at different Td. Although x_j is not correctly known for the cells diffused at 600 and 630 °C owing to the shallow junction or the high background level, x_j can be estimated to be 0.22, 0.34, and 0.46 μm for the cells diffused at 660, 690, and 720 °C, respectively. Figure 5 shows the dependence of solar cell parameters on Td. The open circuit voltage, Voc is almost constant and

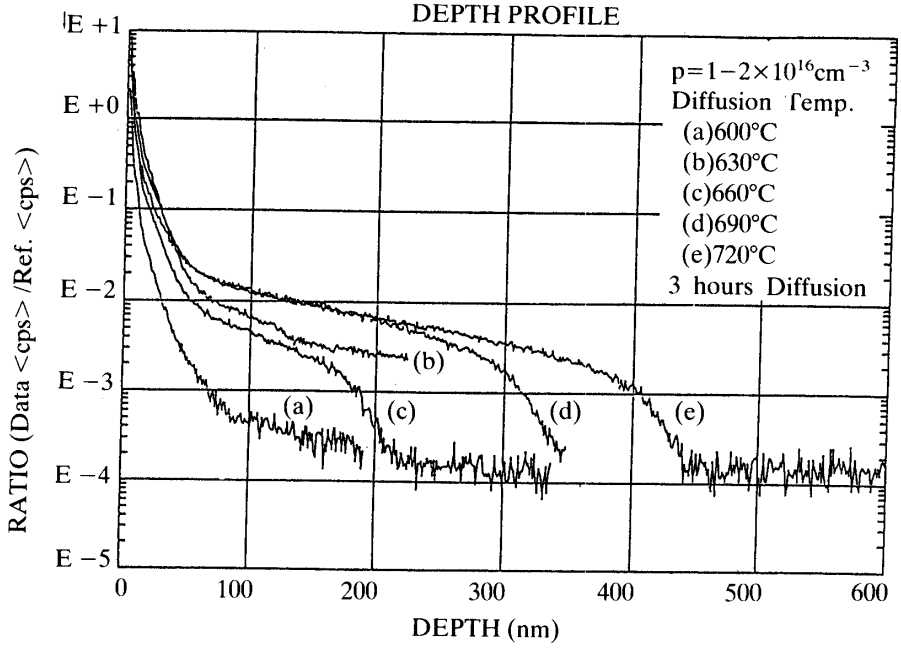

Fig. 4. SIMS profiles of sulfur in cells diffused at different temperature.

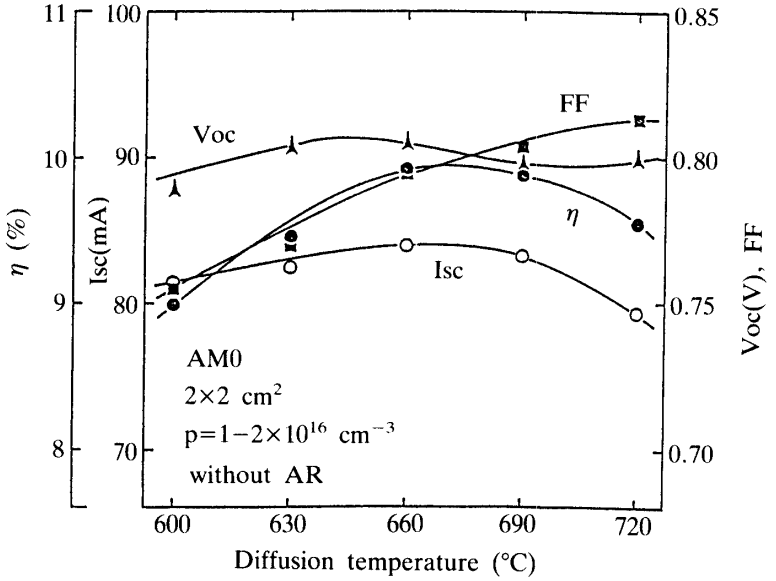

Fig. 5. Dependence of solar cell parameters on diffusion temperature.

independent of Td. The short circuit current, Isc has a peak around 660 °C. Since x_j drastically changes with Td as shown in Fig. 4, this insensitivity of Isc for x_j is rather surprising [*10*]. Figure 6 shows the spectral response of these cells.

We have intensively investigated the influence of the substrate carrier concentation, p on n^+-p junction characteristics and solar cell parameters. Diffusion was performed at 675 °C for 3 hours. Figure 7 shows the depth profiles of the carrier concentration of

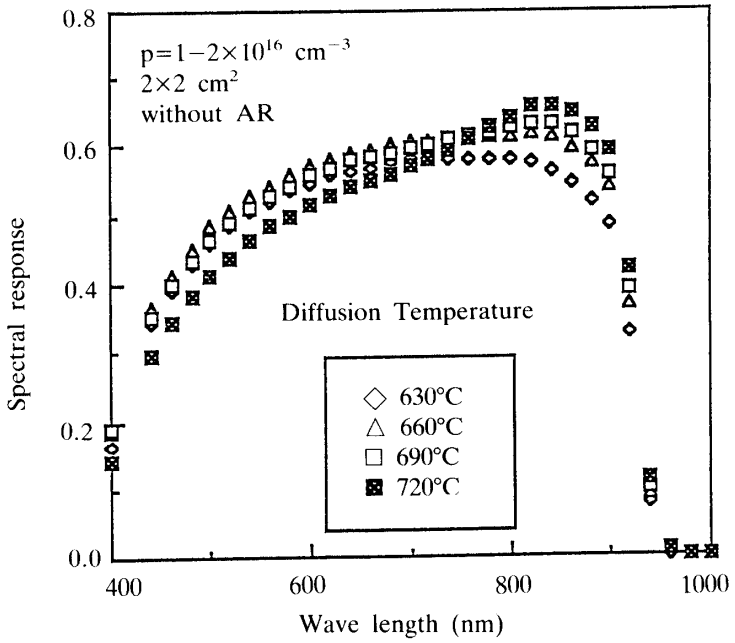

Fig. 6. Spectral response of InP cells diffused at different temperature.

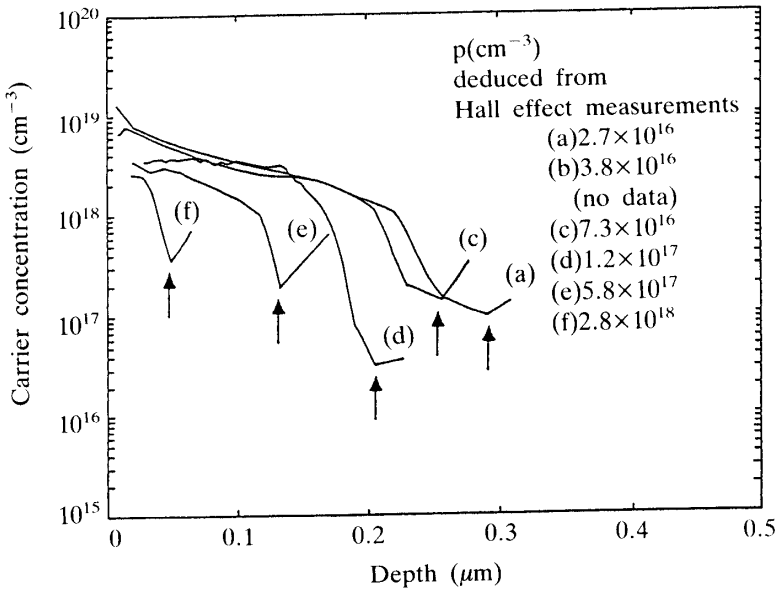

Fig. 7. Carrier concentration profiles of InP cells with different substrate carrier concentration.

the cells with different p, whose profiles were measured by an electrochemical method. The junction depth x_j drastically decreases with increasing p.

Figure 8 shows the dependence of solar cell parameters on p. The open circuit voltage Voc increases up to 10^{17} cm^{-3} reflecting the built-in potential of the n^+-p junction, and then decreases owing to the large decrease in Isc and degradation of the n^+-p junction. The degradation is due to the shallow junction and double doping into

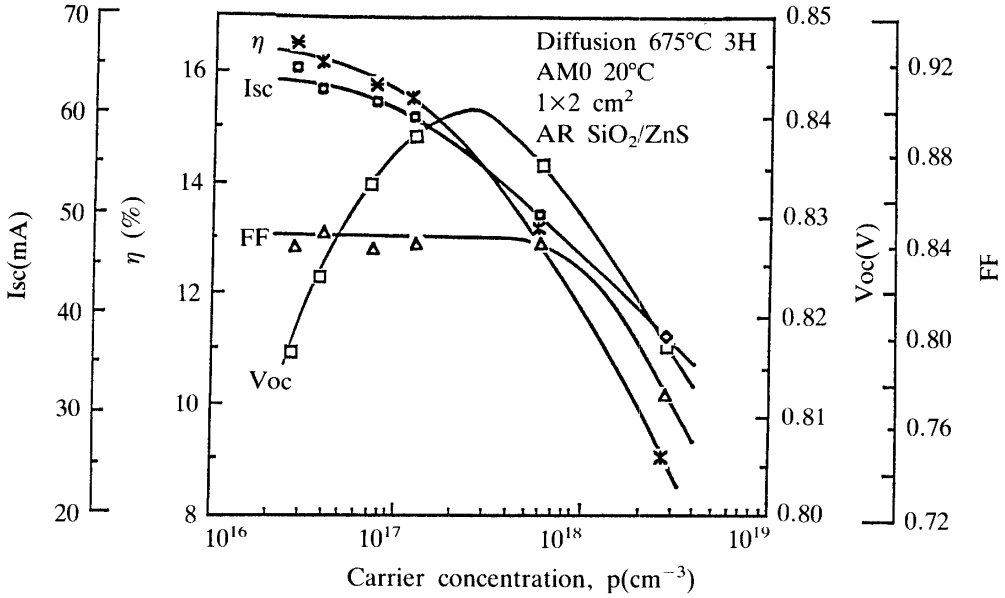

Fig. 8. Dependence of solar cell parameters on substrate carrier concentration.

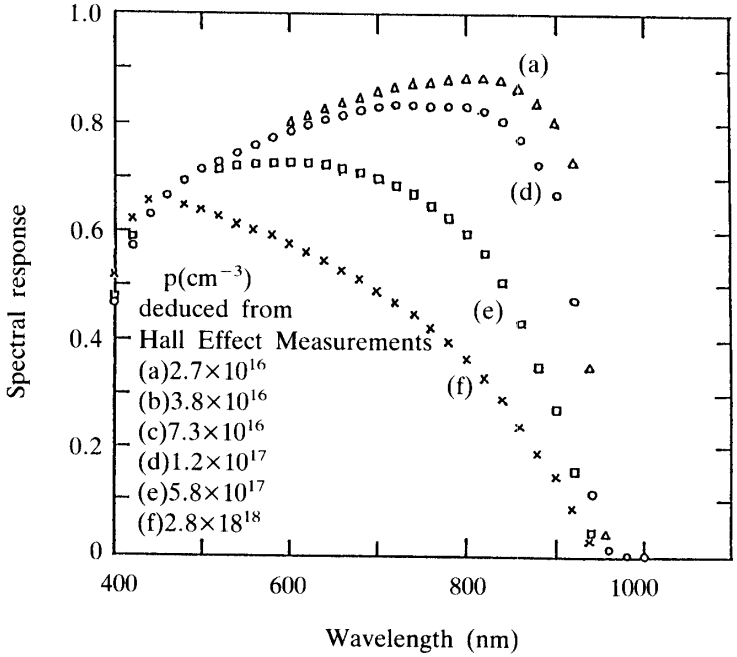

Fig. 9. Spectral response of InP cells with different substrate carrier concentration.

the p type substrate with a high carrier concentration, which increases the recombination in the space charge region and so degrades junction quality.

The fill factor, FF is constant and remains as high as 0.84 up to 6×10^{17} cm^{-3}. It abruptly decreases at 3×10^{18} cm^{-3} of p owing to both a large sheet resistance of the n^+ layer (x_j=0.04 μm) and the degradation of junction quality.

The decrease in Isc is caused by that of the spectral response, SR in the longer wavelength region as shown in Fig. 9. The decrease in the minority carrier diffusion length in the p type substrate with increasing Zn impurities degrades SR in the longer wavelength region. The decrease in x_j with increasing p also degrades SR in the longer wavelength region. As a result of the dependence of Isc, Voc, and FF on p, the conversion efficiency, η slowly decreases with increasing p up to 10^{17} cm^{-3} and then abruptly decreases. Since radiation resistance of InP solar cells increases with increasing p [3], we infer that the optimum p range is 5–10 $\times$ 10^{16} cm^{-3}.

2.2 Electrode Fabrication

After removal of the diffused layer on the rear surface, full-area, back ohmic contacts were formed with vacuum evaporation (0.1 μm in thickness) of Ag-Zn alloy (5 wt.%) followed by annealing at 420 °C for 2 min in flowing H_2 gas. Then, Ag (1 μm in thickness) was electroplated onto the annealed Ag-Zn layer to reduce the series resistance. Front ohmic contacts consist of evaporated Pd (500 Å in thickness) and electroplated Ag (3–5 μm in thickness) which were patterned with conventional lithographic technique. The contact grid lines are 25 μm wide and the spacings between the grid lines are 975 μm. The size of the contact pad is 6 mm $\times$ 1.8 mm; the sum of the electrode area amounts to the shadow loss of about 9 %. No annealing was made for the front contacts. Adhesion of the negative contacts to the n^+ layer has been improved by using Ag/Pd instead of conventional Ag/Pd/Ti. We have confirmed for the first time that this new metal structure of Ag/Pd has excellent reliability for the InP solar cells.

2.3 Mesa-etching

After electrode fabrication, the InP cells were made into mesa-type devices by etching the top edges (20 μm in width) of the cells using photoresist as etching mask. It was found that mesa etching increased cell output despite an active area loss of 0.6 percent.

Figure 10 shows typical Log(I)-V characteristics in the dark for the cells with and without mesa etching. The average solar cell parameters of six cells with and without mesa etching, which were fabricated from one wafer, are summarized in Table 1 with their standard deviation, SD. The large improvement in the ideality factor, n and the reverse saturation, J_0 by mesa etching enables the high values of the voltage Voc and the fill factor FF. Figure 11 shows the spectral response of the cells with and without mesa etching. The spectral response in the shorter wavelength region less than 700 nm is slightly improved by mesa etching.

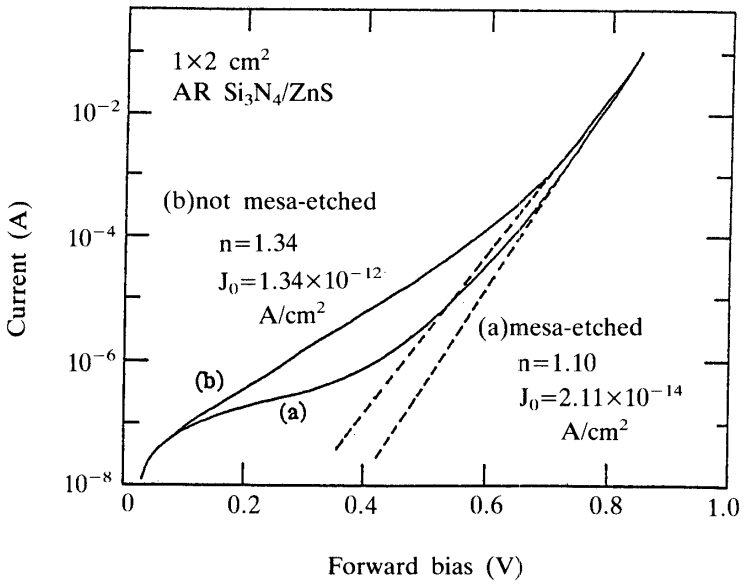

Fig. 10. Typical forward I-V characteristics in the dark for cells with and without mesa etching.

Table 1. Average cell parameters of six cells with and without mesa-etching.

Mesa-Etching	cell no.		Voc (mV)	Isc (mA)	FF (%)	η (%)	n	Jo (A/cm^2)
with	6	Ave.	832	62.2	84.3	16.2	1.12	2.80×10^{-14}
		(SD)	(0.00)	(0.27)	(0.25)	(0.09)	(0.02)	(1.8×10^{-14})
without	6	Ave.	830	61.1	82.4	15.6	1.35	4.93×10^{-12}
		(SD)	(0.47)	(0.31)	(0.33)	(0.10)	(0.05)	(5.8×10^{-12})

* Conditions:
- AM0
- 20°C
- 1×2 cm^2
- AR Si_3N_4/ZnS

2.4 AR Coating Fabrication

Si_3N_4/ZnS were sputtered as antireflection (AR) coating. The AR structure of Si_3N_4/ZnS was selected as it provided maximum efficiency for the cells with coverglass. The AR coating film on the mesa-etched region and the contact pad was removed with lift-off process for the following scribing and welding process.

Figure 12 shows the calculated reflectance as a function of wavelength for Si_3N_4/ZnS coated cells with and without coverglass. The average reflectance between 400 and 900 nm is about 10 % for the cells without coverglass, reducing to about 3 % for the cells with coverglass.

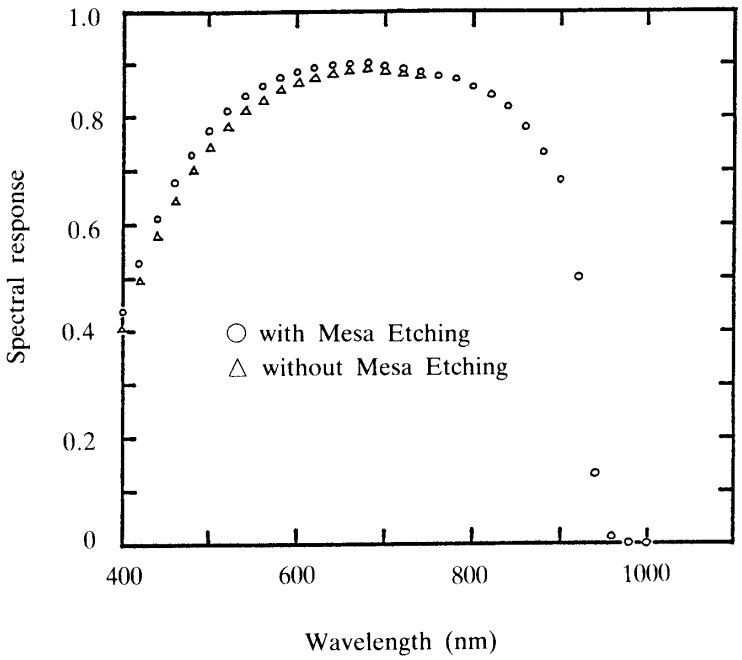

Fig. 11. Spectral response of InP cells with and without mesa etching.

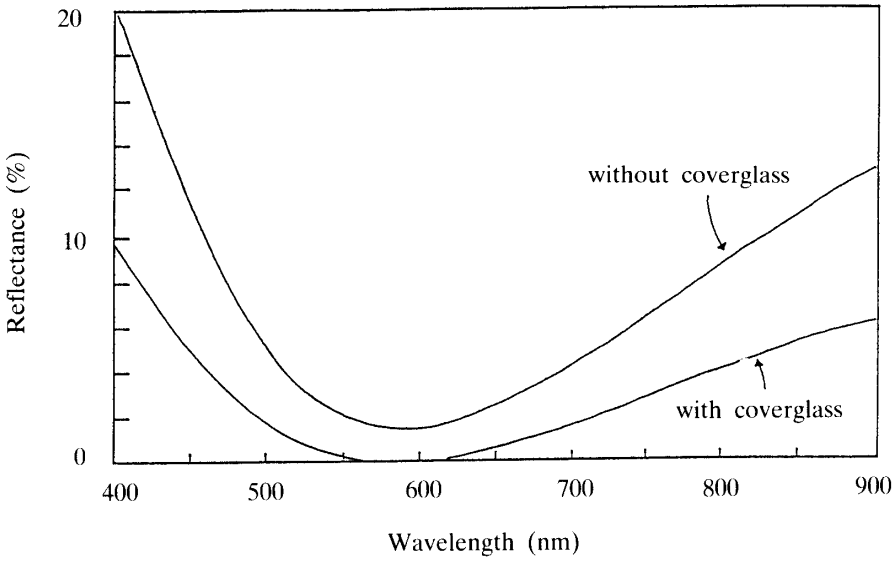

Fig. 12. Calculated reflectance of Si_3N_4/ZnS coated cells with and without coverglass.

2.5 Scribing

After the completion of the above process on wafer, six 1 cm × 2 cm cells were produced from each wafer by scribing along the center of the mesa-etched trenches.

2.6 Welding and Coverglass Installation

Fifty micron thick coverglass made of borosilicate [*11*] was attached on the cells with 30–40 μm thick silicone rubber after welding was performd with the parallel gap welding equipment. The coverglass installation was performed by vacuum adhesion process.

3. Characteristics

In this chapter we describe fundamental electrical and mechanical characteristics and thermal properties of the developed InP solar cells and charged particle radiation effects of InP cells fabricated at NTT Laboratories. Of electrical characteristics, the dependence on the light incident angle and the light intensity is excluded here.

3.1 Electrical Characteristics

The average parameters of 1,080 InP solar cells produced for the lunar orbiter (LO) including the conversion efficiency η, the open circuit voltage Voc, the short circuit current Isc, and the fill factor FF are summarized in Table 2. The distribution of η of 1,000 cells with or without coverglass is shown in Fig. 13. The solar cell parameters were measured under conditions of AM0, 20 °C with a Spectrolab solar simulator (MK-II). Data of our cell characteristics measured at NASA Lewis Research Center were used for calibrating the light source intensity. Figure 14 shows the typical I-V characteristic of a cell for the lunar orbiter.

The temperature dependence of the solar cell parameters was also obtained. The dependence of the maximum output power, Pmax, Voc, and Isc was shown in Fig.

Table 2. Average cell parameters of 1,080 cells with coverglass.

	Cell No.	Voc(V)	Isc(mA)	FF(%)	η(%)
AVE. (S.D.)	1,080	0.828 (0.003)	62.5 (1.2)	83.7 (0.7)	16.0 (0.3)

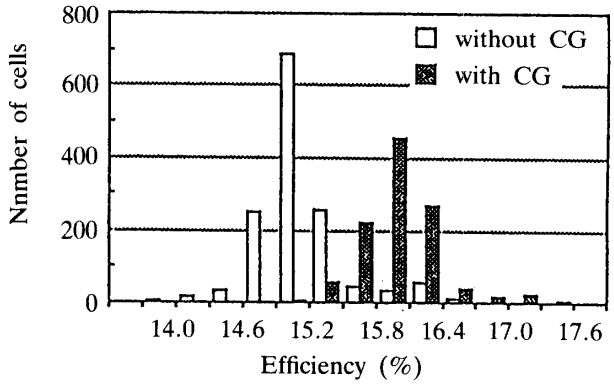

Fig. 13. Conversion efficiency distribution of 1,000 InP cells.

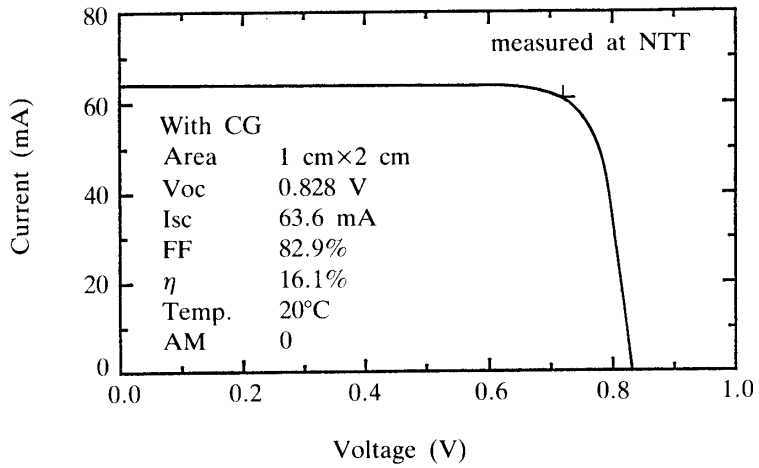

Fig. 14. Typical I-V characteristic of an InP cell with coverglass under illumination.

15(a), (b), and (c). The temperature coefficients of those parameters were -0.10 mW/cm^2 °C, -1.84 mV/°C, and 0.09 mA/cm^2 °C, respectively.

3.2 Thermal Properties

Operating temperature of solar cells in space is important for power generated during projected lifetime of satellites because the cell maximum power depends strongly on their temperature. The operating temperature is mainly determined by two thermal parameters: solar absorptance and total hemispherical emittance of cells. It is well known that these parameters tend to vary with elapsed time in orbit. From this point of view, thermal properties of the InP solar cells must be investigated quantitatively. Thus, the solar absorptance, α_S and the total hemispherical emittance, ϵ_H of the InP cells have been obtained with our simultaneous measurement [*12, 13*]. Principle for the measurement is shown in Fig. 16. The solar radiation of the intensity, S illuminates a test sample vertically, and the sample temperature in equilibrium, Ts_0 is measured. In the next step, sample temperatures, Ts_1 and Ts_2 corresponding to two input levels of heater power, P_1 and P_2 are measured under the above solar radiation. In this case, three sets of thermal balance equations on α_S and ϵ_H are given as follows:

$$SA\alpha_S = A\epsilon_H \sigma Ts_0^4 + K(Ts_0 - T_{B0}),$$

$$SA\alpha_S + P_1 = A\epsilon_H \sigma Ts_1^4 + K(Ts_1 - T_{B1}),$$

$$SA\alpha_S + P_2 = A\epsilon_H \sigma Ts_2^4 + K(Ts_2 - T_{B2}),$$

where A is the sample area, K the heat conductance of thermal insulation, σ Stefan Boltzmann constant, and T_{B0}, T_{B1}, and T_{B2} each equilibrium temperature of a base plate under solar radiation and heat power inputs, respectively. Solving these simultaneous equations, we can obtain the parameters α_S, ϵ_H, and K by the following equations.

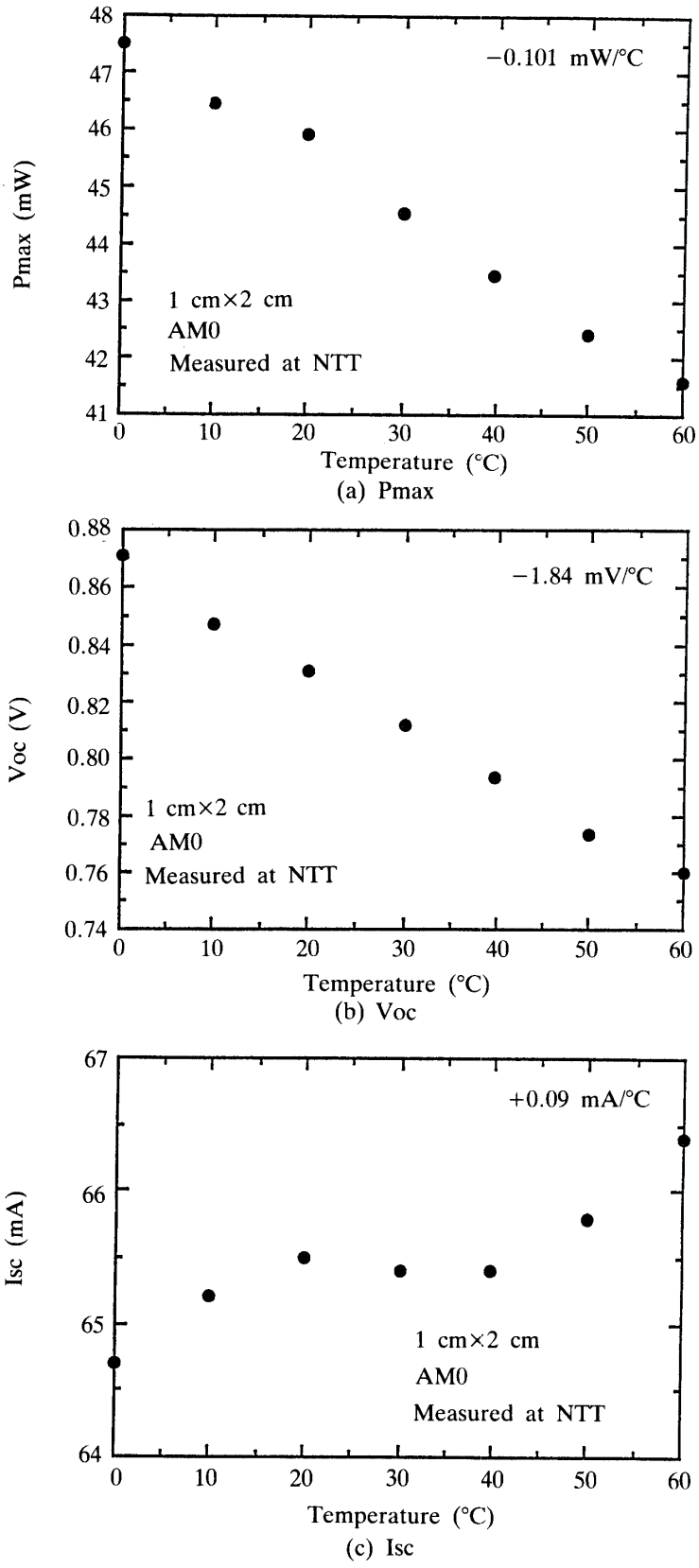

Fig. 15. Temperature dependence of maximum output power, open circuit voltage, and short circuit current.

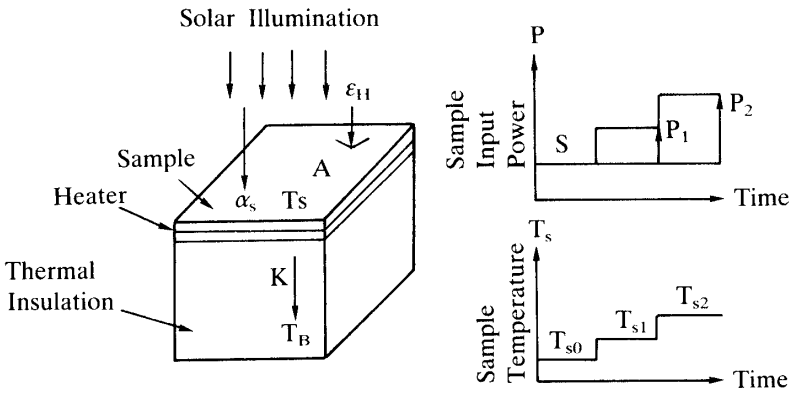

Fig. 16. Principle for measurement.

$$K=\frac{P_1(Ts_2^4-Ts_0^4)-P_2(Ts_1^4-Ts_0^4)}{\Delta_1(Ts_2^4-Ts_0^4)-\Delta_2(Ts_1^4-TS_0^4)},$$

$$\alpha s=\frac{Ts_0^4P_1-K(\Delta T_1Ts_0^4-\Delta T_0Ts_1^4)}{SA(Ts_1^4-Ts_0^4)},$$

$$\epsilon_H=\frac{P_1-K(\Delta T_1-\Delta T_0)}{A\sigma(Ts_1^4-Ts_0^4)},$$

$$\Delta T_0=Ts_0-T_{B0},$$

$$\Delta T_1=Ts_1-T_{B1},$$

$$\Delta T_2=Ts_2-T_{B2},$$

$$\Delta_1=\Delta T_1-\Delta T_0,$$

$$\Delta_2=\Delta T_2-\Delta T_0.$$

The following assumptions are adopted here: i) the temperature dependence of ϵ_H can be neglected within the sample temperature change, ΔTs ($=Ts_1-Ts_0$) and ii) the heat loss through the side surface of the thermal insulation block is negligible.

The thermal properties of the InP solar cells without coverglass are shown in Table 3 along with those of Si cells with ITO coated coverglass of 50 μm in thickness. As was expected that from the ratio, α_s/ϵ_H obtained in Table 3, the InP cells show higher temperature in orbit than the Si cells do, the InP cell temperature on flight data obtained from an absorptance/emittance measurement on board the twelfth satellite was actually higher by 15°C and showed 100°C during the sunlit period in orbit.

Table 3. Thermal property data of solar cells.

Sample	α_s	ϵ_H	Abbreviation
ITO/Coverglass (50 μm)/Si Solar Cell	0.73	0.79	Si
Antireflection/InP Solar Cell	0.83	0.57	InP

We can apply the above method to the measurement of thermal properties of other surface materials even in space.

3.3 Mechanical Characteristics

As mechanical failure states of the solar cell itself, the following are considered.

1) Crack
2) Chip
3) Nick
4) Electrode delamination
5) Antireflection coating film delamination

The above defects can result in part of the factors of cell electrical performance degradation. Especially under environments such as shock and vibration during launch period and ultraviolet ray and charged particle irradiation and thermal cycling in orbit, solar cells for scientific satellites are required not to cause the above mechanical defects.

In general, it seems that InP solar cells are brittler than Si cells in mechanical intensity. Because of this confirmation, mechanical intensity of an InP cell was measured in two ways: compression and three point bending methods. The configuration for the measurement is shown in Fig. 17(a) and (b). The measured result is shown in Table 4 including that of a Si cell of 280 μm in thickness. From this table, it is found that the InP cell is able to withstand about 60 % smaller load than the Si

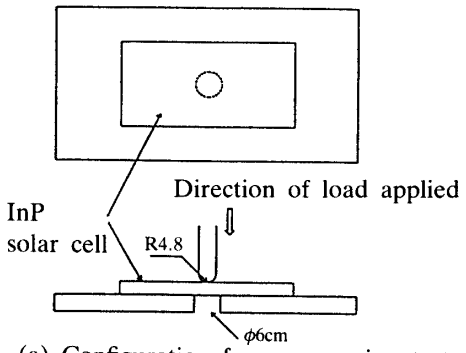

(a) Configuration for compression test

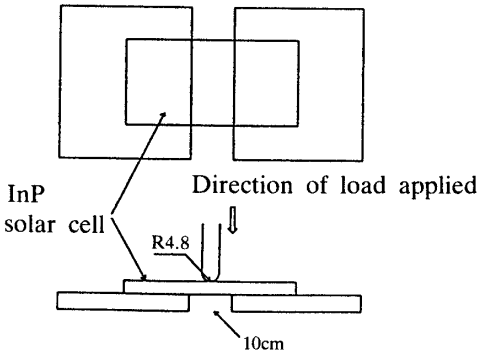

(b) Configuration for three point bending test

Fig. 17. Configuration for mechanical intensity measurement.

Table 4. Measured results of mechanical intensity.

No	InP Cell (400 μm thick)		Si Cell (280 μm thick)	
	Compression Test	Three Point Bending Test	Compression Test	Three Point Bending Test
1	2.80 kg	1.16 kg	5 kg over	4.77 kg
2	2.24	1.74	"	2.16
3	3.08	1.48	"	3.55

cell.Besides, as destroyed circumstances the Si cell was broken radially and the InP cell was cracked linearly. Generally the brittleness of solar cells depends considerably on the plane orientation of their substrates. We can expect more improvement in the mechanical intensity of the InP cells by using the substrates with off-cut plane instead of such low index plane.

From the viewpoint of the above mechanical intensity, the protection against chip, nick and so on, and the ease of surface cleaning on InP cells, it is thought it is essential for the LO cells to install coverglass on them. Thus, 50 μm thick coverglass was adopted. As a result, the weight allocation for an LO cell is shown in Table 5.

Table 5. Weight allocation of an InP solar cell.

Constituent elements	Weight (g)
Cell (1×2 cm^2)	0.380
Coverglass	0.026
Adhesive	0.022
Interconnector	0.011
Total	0.439

3.4 Charged Particle Irradiation Effects

In this section, the mechanism of radiation resistance of InP solar cells mainly with 1 MeV electron irradiation already studied in DLTS (Deep Level Transient Spectroscopy) method, etc. is reviewed by comparing irradiation effects on InP cells with those of GaAs and Si cells [*14*].

3.4.1 Radiation Resistant Characteristics of InP Solar Cells

As a result of the evaluation of the effects of Co^{60} gamma ray and 1 MeV electron irradiation on n^+-p junction InP solar cells [*2, 3*], Yamaguchi et al. have found that InP solar cells are superior to Si or GaAs cells in radiation resistance. Figure 18 shows changes in relative conversion efficiency of InP solar cells with various kinds of

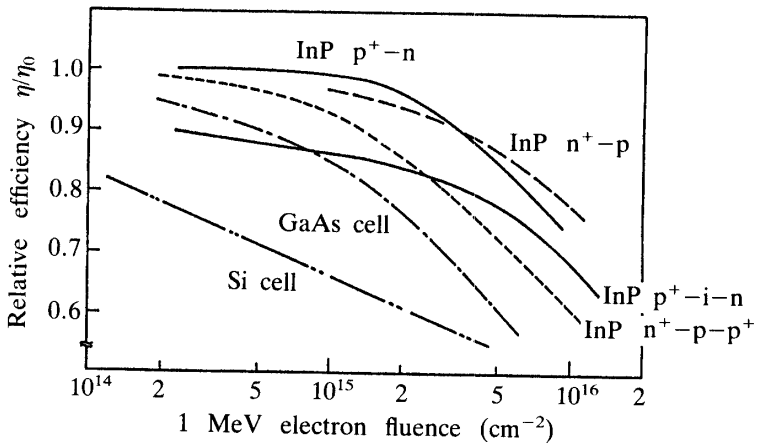

Fig. 18. Changes in air mass 1.5 relative conversion efficiency for InP solar cells with various structures, Si, and GaAs solar cells as a function of 1 MeV electron fluence.

structures under 1 MeV electron irradiation in comparison with those of Si and GaAs cells. In the cells with the structures studied, it is found that their conversion efficiency is maintained high even at higher irradiation fluences and that the InP cells are much more resistant to radiation than Si or GaAs cells. The radiation resistance precedence for the cell structures is as follows:

$$p^+-n=n^+-p-p^+>n^+-p>p^+-i-n.$$

Figure 19 shows that the radiation degradation of the InP solar cells is due mainly to the decrease in the short circuit current resulting from the degradation of the minority carrier diffusion length based on lattice defects (i.e., recombination centers) introduced by irradiation. At higher irradiation fluences, it is found that a rapid decrease in FF is caused by the increase in the series resistance due to the decrease in the majority carrier concentration by means of trap centers. As shown in Figs. 20 and 21, changes in the minority carrier diffusion length and the majority carrier

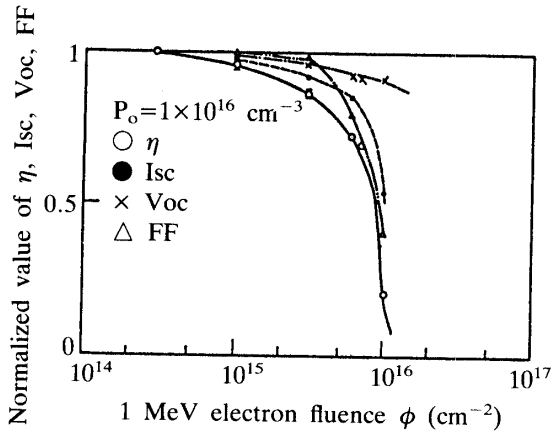

Fig. 19. Changes in relative cell parameters for a n^+-p junction InP soar cell as a function of 1 MeV electron fluence.

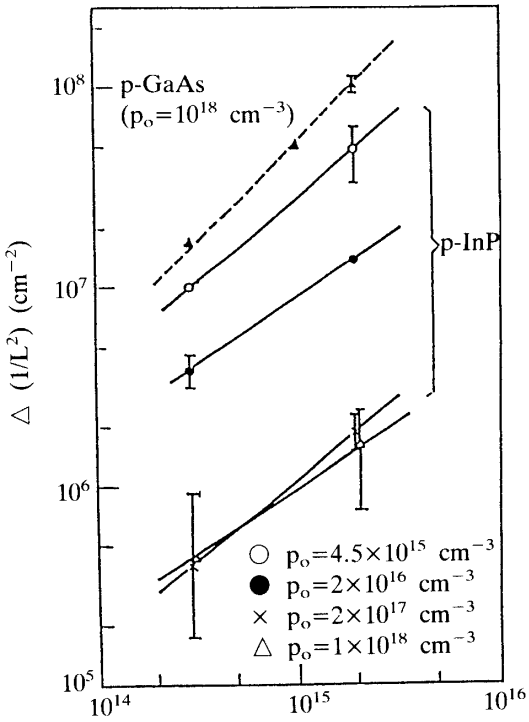

Fig. 20. Changes in inverse square of diffusion length $\Delta(1/L^2)$ for p type InP with various carrier concentrations as a function of 1 MeV electron fluence in comparison with that in p type GaAs.

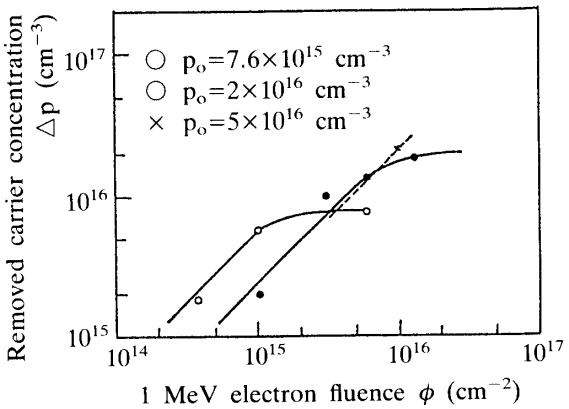

Fig. 21. Changes in carrier removal Δp in p type InP with various carrier concentrations as a function of 1 MeV electron fluence.

concentration with 1 MeV electron irradiation cause the decrease in the short circuit current density J_{sc}, Voc, FF, etc. These can be seen from the following equations.

$$J_{sc}=qgL, \tag{1}$$

$$1/J_{sc\phi}{}^2-1/J_{sc0}{}^2\propto 1/L_\phi{}^2-1/L_0{}^2=\sigma Nrv/D, \tag{2}$$

$$Voc=(nkT/q)\ln(J_{sc}/J_0+1), \tag{3}$$

$$J_{0\phi}-J_{00}=qn_iWD(1/L_\phi^2-1/L_0^2)=qn_iW\sigma Nrv, \tag{4}$$

$$FF=f(Rs), \tag{5}$$

$$Rs_\phi-Rs_0=(1/q\mu)(1/N_\phi-1/N_0)$$
$$=(1/q\mu)Nmaj/N_0(N_0-Nmaj), \tag{6}$$

where the suffixes, 0 and ϕ mean before and after irradiation. q, g, and σ are electronic charge, the generation rate of hole-electron pairs due to incident light, and the capture cross section for a minority carrier, respectively. Nr is the number of recombination centers introduced by irradiation, v is the thermal velocity of the minority carrier, D is the diffusion coefficient of the minority carrier, n is the diode factor, k is Boltzmann's constant, T is the absolute temperature, J_0 is the dark current density, n_i is the intrinsic carrier density, W is the width of the depletion region, Rs is the series resistance for a solar cell, μ is the carrier mobility, and Nmaj is the number of majority carrier trap centers introduced by irradiation.

The p^+-n type cells can suppress the increase in the series resistance caused by irradiation in the case of using n type substrates and are superior in radiation resistance. The n^+-p-p^+ type cells have the same property as the p^+-n type cells by introducing p^+ layers. On the one hand, the carrier generation recombination current due to recombination centers generated in i layers by irradiation increases in the p^+-i-n type cells. The decrease in Voc is also caused as shown in Fig. 22. From the viewpoint of efficiency and radiation resistance for the p^+-i-n cells, the optimum thickness of the i layers ranges from 0.5 to 1 μm as shown in Fig. 23.

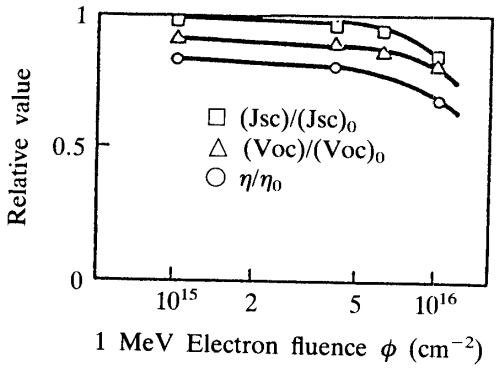

Fig. 22. Changes in cell parameters of InP solar cells with p^+-i-n structure under electron irradiation.

Recently, Weinberg et al. [*15*] have also studied the effect of 10 MeV proton irradiation on InP solar cells and confirmed their superior radiation resistance. Figure 24 compares the 10 MeV proton irradiation effect of InP cells with n^+-p junctions (made in NTT) with that of GaAs cells with n^+-p junctions (made in MIT) and Si cells with n^+-p junctions and back surface reflectors (made in Spectrolab). It is found that

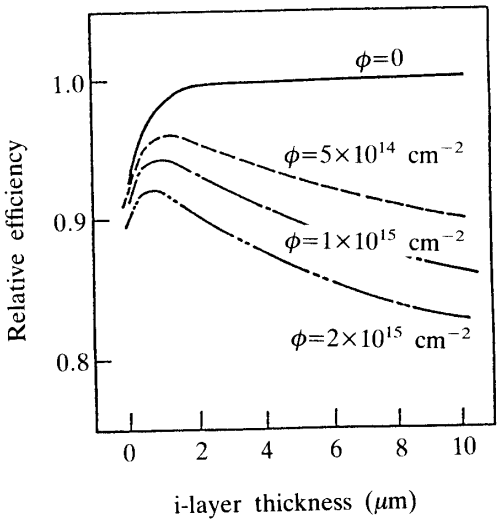

Fig. 23. Numerical analysis results of dependence of normalized efficiency of InP cells with p^+-i-n structure on i layer thickness under electron irradiation.

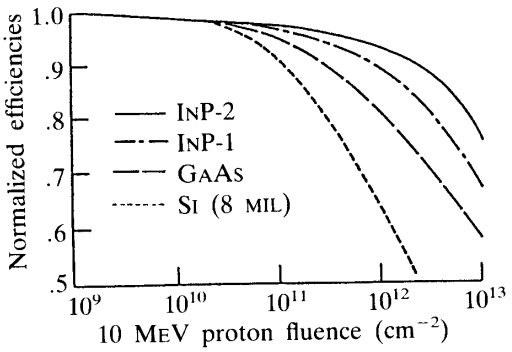

Fig. 24. Normalized efficiency of 10 MeV proton irradiated InP, Si, and GaAs solar cells.

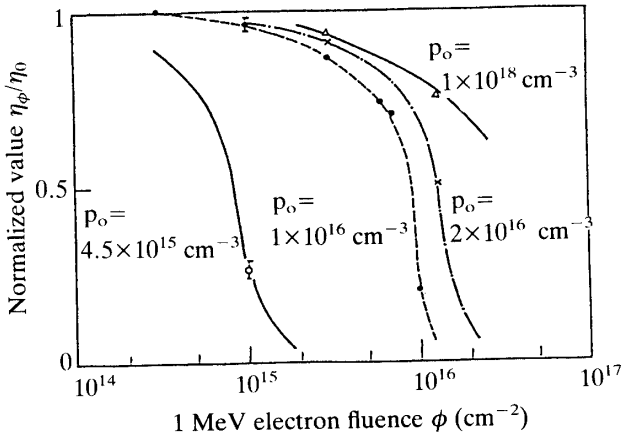

Fig. 25. Normalized conversion efficiency for n^+-p junction InP solar cells with various substrate carrier concentrations with 1 MeV electron irradiation.

InP cells are resistant to proton irradiation as well as gamma ray and electron irradiation.

Figure 25 shows the dependence of electron irradiation characteristics of the InP cells with n^+-p junction on the carrier concentration in p type substrates [*3*]. One of the features of these irradiation characteristics is to be more resistant to the above electron irradiation, as the carrier concentration in the InP substrates becomes higher. This is because the decrease in the minority carrier diffusion length and the majority carrier concentration under irradiation is suppressed with increasing impurity concentration in the substrates as shown in Figs. 26 and 27.

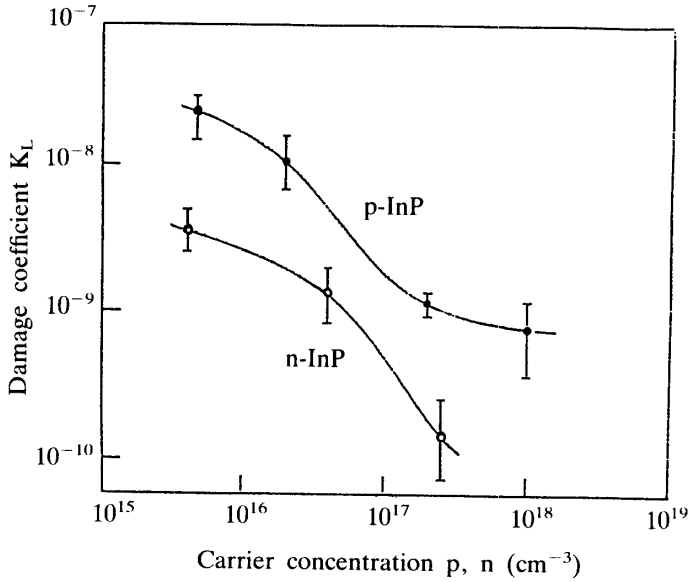

Fig. 26. Changes in damage coefficients for diffusion length K_L in InP, GaAs, and Si determined with 1 MeV electron irradiation as a function of material carrier concentration.

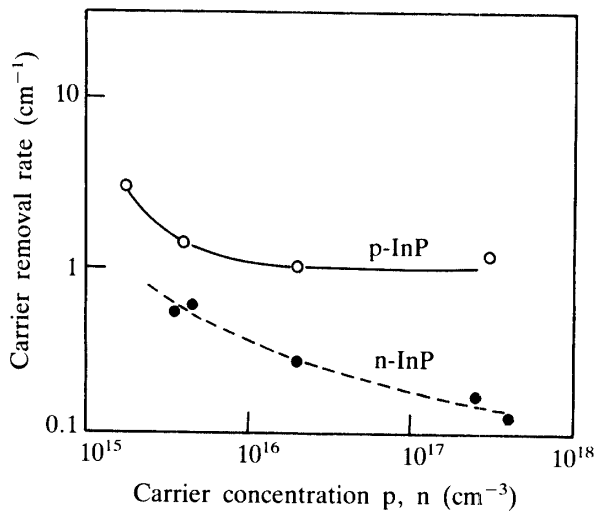

Fig. 27. Dependence of carrier removal rate on InP single crystal carrier concentration under 1 MeV electron irradiation.

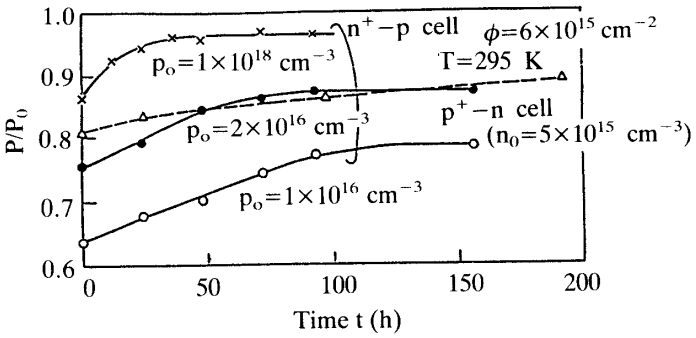

Fig. 28. Maximum power recovery due to room temperature annealing for 1 MeV electron irradiated InP solar cells with various substrate carrier concentrations.

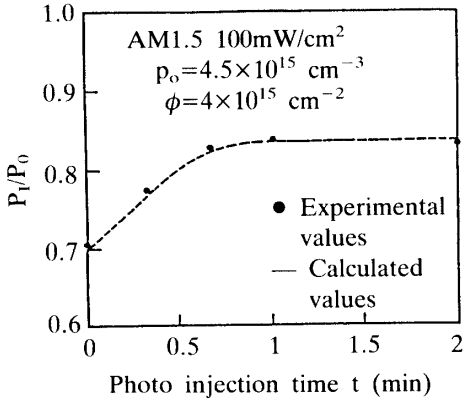

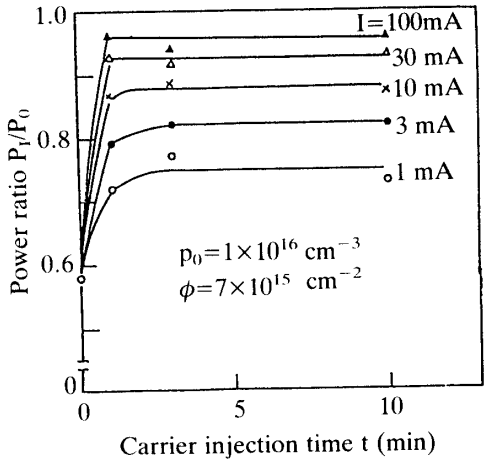

Fig. 29. Maximum power recovery due to photoinjection using air mass 1.5 solar simulator and forward bias injection for n^+-p junction InP solar cells after 1 MeV electron irradiation.

Besides, Yamaguchi et al. have found the following interesting phenomena on radiation damage behaviors of the InP cells.

1) Radiation-induced defects in the InP cells are readily mobile at room temperature and annihilate according to the following equation; the InP cells recover from radiation damage even under room temperature exposure as shown in Fig. 28 [*4*].

$$Nd=Nd_0\exp(-At_a), \tag{7}$$

where Nd is the defect concentration, Nd_0 is the initial defect concentration, A is the annealing rate, and t_a is the annealing time. It has been found that such annealing effect of radiation-induced defects is observed in both n type InP and p type InP materials and that annealing rate increases with increasing carrier concentration. The room-temperature recovery phenomena of radiation-induced defects in the InP cells are not observed in GaAs cells [*16*].

2) InP cell characteristics degraded by irradiation readily recover with minority carrier injection by means of light illumination and forward bias application as shown in Fig. 29. The reason is as follows: the annealing rate under minority carrier injection, A^* is increased by 6–7 orders of magnitude compared with the thermal annealing rate in Eq. (7) and radiation-induced defects rapidly annihilate, so that the minority carrier diffusion length mainly recovers. However, this annealing phenomenon with minority carrier injection is more remarkable in the n^+-p cells than in the p^+-n cells. Moreover, this phenomenon at room temperature is not observed in GaAs cells.

3) In relation to the phenomenon 2), the radiation degradation of the InP cells by irradiation under solar cell operation was decreased compared with that under no operation as shown in Fig. 30 [*17*]. The reason is considered as follows: rapid

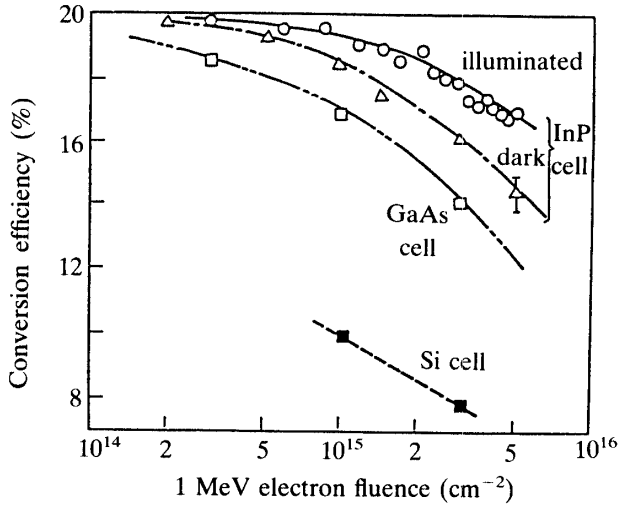

Fig. 30. Changes in air mass 1.5 conversion efficiency for n^+-p junction InP solar cells under light illumination or dark condition as a function of 1 MeV electron fluence in comparison with radiation effects for Si or GaAs solar cells.

radiation-induced defect annihilation due to the annealing rate enhanced with minority carrier injection (A*) is caused together with defect generation by irradiation and the degradation of the minority carrier diffusion length is mainly prevented as shown in the following equation.

$$\Delta(1/L^2)=1/L_\phi{}^2-1/L_0{}^2$$
$$=(K_L f/A^*)\{1-\exp(-A^* t)\}, \tag{8}$$

where K_L, f, and t are the damage coefficient, the irradiation flux, and the irradiation time, respectively. As a result, the decrease in the short circuit current is alleviated. This phenomenon is also considered peculiar to InP cells.

3.4.2. Difference Between Radiation Resistance Characteristics of Si Solar Cells and Compound Semiconductor Cells

The reason why Si solar cells are less resistant to radiation than compound semiconductors like GaAs and InP cells is not because the introduction rate of radiation-induced defects in Si semiconductors is larger than that of compound semiconductors. We discuss the difference between both introduction rates.
Generally, one of the factors of solar cell characteristic degradation is the decrease in the minority carrier diffusion length. The change in inverse square of the diffusion length, $\Delta(1/L^2)$ and the irradiation fluence ϕ are related with the following equation.

$$\Delta(1/L^2)=1/L_\phi{}^2-1/L_0{}^2$$
$$=\Sigma\Delta(E_B)_i\sigma_{Ci}v\phi/D=K_L\phi, \tag{9}$$

where $\Delta(E_B)_i$ is the probability that an incident particle produces the i-th recombination center (radiation-induced defect), σ_{Ci} is the capture cross section for the minority carrier.

Then, We can compare K_L of Si in Eq. (9) with that of compound semiconductors and investigate the difference between the radiation-induced defect introduction rates for both semiconductors.

Figure 31 shows changes in the damage coefficient K_L with 1 MeV electron irradiation in p type InP crystals together with Si and compound semiconductor crystals [*18–20*]. The damage coefficient K_L in the p type InP crystals becomes smaller with increasing carrier concentration, which is regarded as a proof of the dependence of radiation damage chracteristics on the carrier concentration in the InP solar cell substrates in Fig. 25. As mentioned later, this reflects the dependence of the room temperature annealing rate for radiation-induced defects on the impurity concentration in the InP crystals. A higher impurity concentration in the crystals results in a larger annealing effect and a smaller damage coefficient at room temperature. In contrast with this, the Si and the GaAs crystals show a counter tendency since the latter damage coefficient becomes larger with increasing carrier concentration. As already known, radiation-induced point defects such as interstitial atoms I and

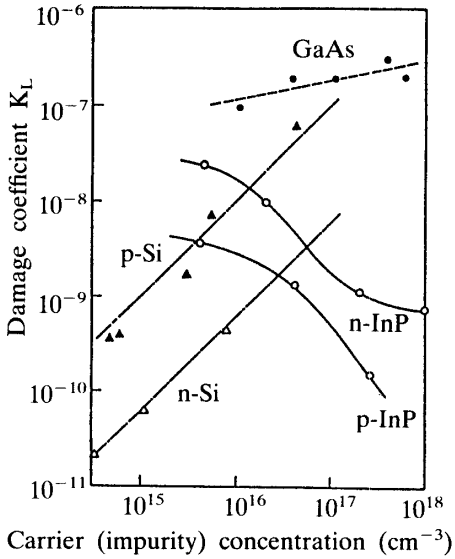

Fig. 31. Changes in damage coefficient for diffusion length in InP, Si, and GaAs crystals with 1 MeV electron irradiation as a function of carrier concentration.

vacancies V in Si crystals annihilate at a low temperature less than 150 K and defects observed at room temperature have vacancy-impurity complex structure like V-O, V-P, and V-B. Therefore, the room temperature damage coefficient tends to increase with increasing carrier (impurity) concentration in Si crystals. In addition, as to the dependence of the damage coefficient on the carrier concentration in GaAs crystals, their radiation-induced defects do not mean the same complex defects combined with impurities as those of Si crystals. As shown in the following equations, the dependence reflects that the position of Fermi level, E_F moves as the carrier concentration varies and that a probability at which the recombination centers with the energy level, Er_i capture a minority carrier changes.

$$\Delta(1/L^2)=\Sigma(E_B)_i\sigma_i f(Er_i)v\phi/D, \tag{10}$$

$$f(Er_i)=\exp[(E_F-Er_i)/kT],\ E_F<Er_i \tag{11}$$

$$f(Er_i)=1,\quad E_F\geq Er_i. \tag{12}$$

From Fig. 31, it is shown that the radiation-induced defect introduction rate for InP crystals is lower than that of GaAs crystals and that InP crystals have superior radiation resistance. However, the introduction rate for compound semiconductors is not always lower than that of Si crystals.

The fact that compound semiconductor solar cells are superior to Si cells in radiation resistance is due to the difference of the energy band structure for these materials as shown in Fig. 32. In this figure, we assume that a distribution for the light-induced carrier density collected at the surface junction in Si and III-V compound semiconductors is expressed by $\alpha \cdot \exp(-\alpha x) \cdot \exp(-x/L)$. It can be seen that those compound semiconductors seldom suffer a decrease in the spectral

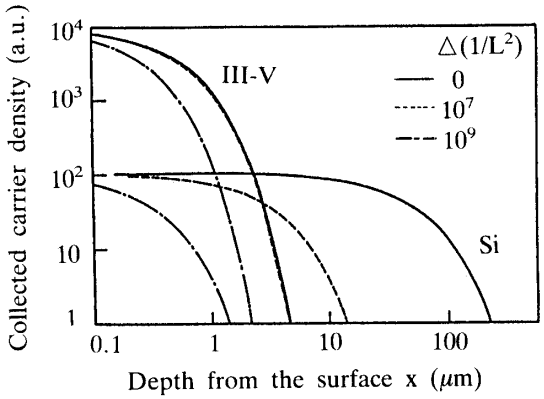

Fig. 32. Plots of collected carrier density n_{ph} for Si and III-V compound semiconductors as functions of depth from the surface and defect introduction $\Delta(1/L^2)$.

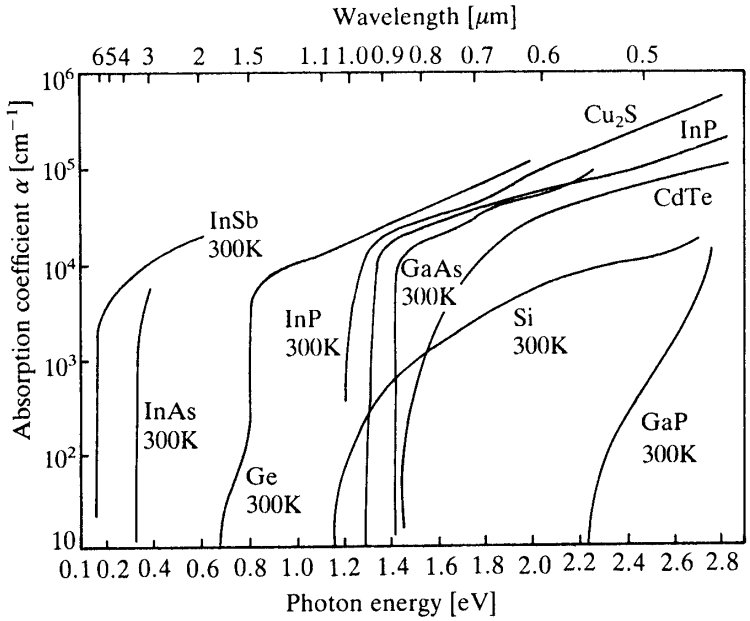

Fig. 33. Absorption coefficients of typical semiconductors.

response by irradiation. Such semiconductors as InP and GaAs crystals have the direct band-gap structure and the absorption coefficient, α of 10^4 to 10^5 cm^{-1} as shown in Fig. 33 [*21*]. The active region for those solar cells is shallow, namely in the range between 1 and 3 μm from their surface. Moreover, their minority carrier diffusion lengths are short and range from 3 to 10 μm.

On the one hand, the spectral response of Si crystals with the indirect band-gap structure decreases very remarkably by irradiation; Si crystals have the absorption coefficient of 10^2 to 10^3 cm^{-1} and the longer minority carrier diffusion length of about 100 μm, requiring the active region from 100 to 300 μm.

Figure 34 shows a calculation example on the effect of the number of radiation-induced defects on the short circuit current in Si and compound semiconductors. As shown in Fig. 32 as a model illustration, it is impossible for compound semiconductor

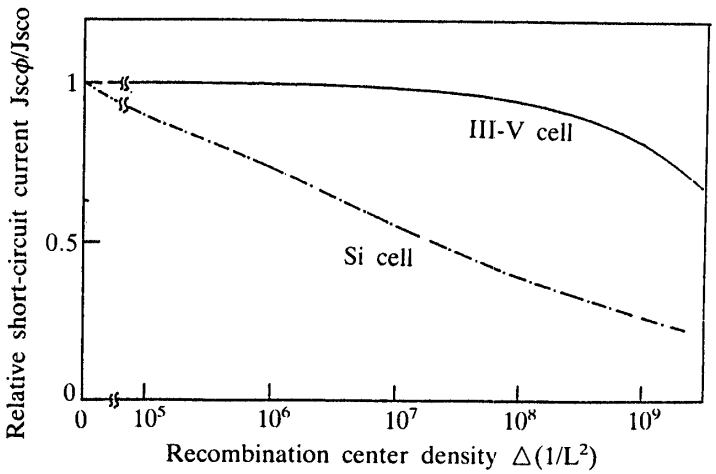

Fig. 34. Numerical analysis results for changes in short circuit current density for Si and III-V compound cells as a function of radiation-induced recombination center density.

solar cells to suffer the degradation of their characteristics due to irradiation although they have more defects than Si cells by two orders of magnitude. Si solar cells are worse than GaAs cells in radiation resistance in spite of the fact that the radiation-induced defect introduction rate for Si crystals is lower than that of GaAs crystals as shown in Fig. 31. InP cells have radiation resistance superior to that of GaAs cells since the defect introduction rate for InP crystals is lower than that of GaAs crystals.

From the above discussion, it is found that the difference between radiation resistance characteristics on Si and compound semiconductor solar cells is not due to the difference between the introduction rates of radiation-induced defects but due to the difference between both semiconductors in the energy band structure.

4. Environmental Tests

Space solar cells mounted on the scientific satellites must maintain their reliable performance in severe space environments during a long-term period of time. In order to evaluate the developed InP solar cells under such requirements, we conducted ground tests that simulated a vibration environment during the launch period and thermal cycling, ultraviolet ray, and proton and electron irradiation environments in orbit. We carried out not only the above tests but also other tests of the cells, but exclude detailed description of the latter tests except an electrode pull strength one.

4.1 Electrode Pull Strength Test

After welding of their interconnectors, pull strength of the front and back electrodes of the InP solar cells was measured with a pulling equipment. A 45 degree pulling test of the interconnectors was performed at a pull speed of 4 mm/min. The test was evaluated with different welding parameters that included applied voltage,

Table 6. Welding parameters of cell electrodes.

WELDING PARAMETER \ No.	1	2	3	4	5	6	7	8
APPLIED VOLTAGE (V)	1.25	1.25	1.0	1.0	1.25	1.25	1.25	1.25
APPLIED TIME (cycle)	4	4	6	7	5	6	4	3
CURRENT CONTROL (%)	70	50	70	50	50	50	60	50
NUMBER OF CONTACT POINTS	4	4	4	4	4	4	4	4

Table 7. Pull strength test results of electrodes.

ELECTRODE	FRONT CONTACT		BACK CONTACT
WELDING PARAMETER	Ag/Ti/Pd	Ag/Pd	Ag/Zn
1	203(1)		
2	168(4)	933(13)	404(1)
3	189(4)	808(13)	
4	88(1)		
5	140(2)	740(4)	603(2)
6			505(2)
7			810(2)
8			918(2)
SOLDERING	273(2)		1460(1)

applied time, current control rate, and the number of contact points shown in Table 6. Pull strength difference between new Ag/Pd structure and conventional Ag/Ti/Pd structure for front contacts was also investigated. The test results are shown in Table 7. With the Ag/Pd structure, sufficient pull strength was obtained. The applied voltage and the time for welding were determined at the lowest value enough to protect the degradation of junction quality in case of an excess applied voltage or time because such degradation decreased FF. Therefore, the welding parameters of No. 3 for front contacts and No. 8 for back contacts were adopted for the production of the cells for the lunar orbiter.

A temperature cycling test was also conducted up to 21 cycles. In one cycle, the cell temperature ranged from −70 °C to 70 °C in 140 minutes. No change in pull strength was observed before and after the test.

4.2 Vibration and Thermal Cycling Tests

In order to confirm resistance of the InP solar cells to the severe environments of vibration during launch period and thermal cycling in orbit, these environmental tests were carried out by mounting the InP cells on a honeycomb substrate for the lunar orbiter.

4.2.1 Thermal Cycling Test

A samlpe shown in Fig. 35 was fabricated and subjected to a thermal cycling test up to 100 cycles. As seen from a temperature profile in Fig. 36, the sample was held for 10 minutes at each temperature of −120 and 100 °C. A visual inspection and an electrical performance test were conducted before and after this cycling test. There was no change in the inspection and performance test results.

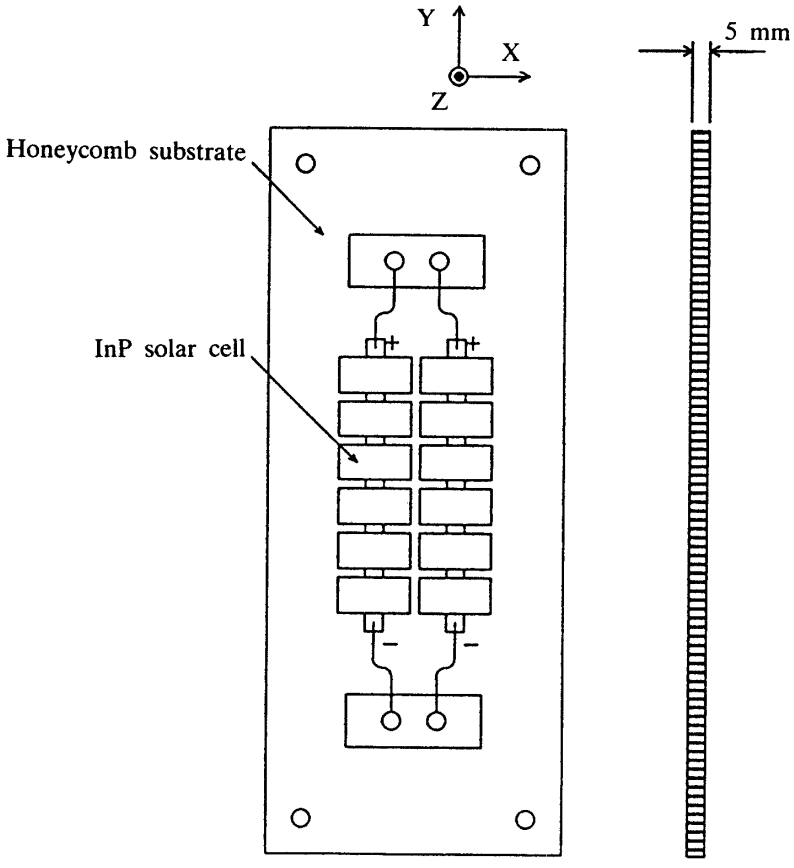

Fig. 35. Sample of thermal cycling and vibration tests.

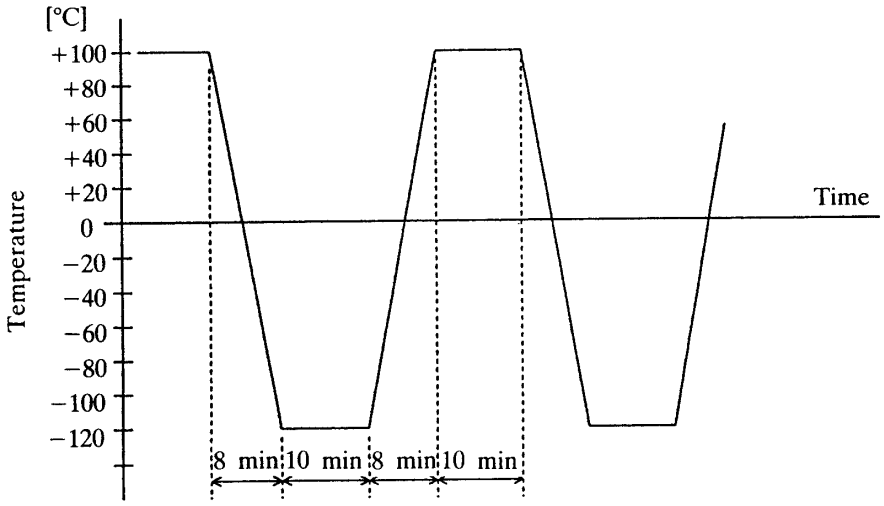

Fig. 36. Temperature profile of thermal cycling test.

4.2.2 Vibration Test

A vibration test was conducted with the same sample as the thermal cycling test. The test was divided into three steps: (i) random vibration at acceptance level for the thirteenth scientific satellite, (ii) sinusoidal vibration up to destruction, and (iii) sinusoidal resonance up to destruction.

Random vibration test level is shown in Table 8. During vibration, the short circuit current of the sample was monitored with a simple light source.

As shown in Fig. 37, a sinusoidal vibration test at a constant acceleration of 50 or 60 G was carried out by sweeping the frequency range from 5 to 2,000 Hz in 5 minutes. The short circuit current was also monitored during the test.

A sinusoidal resonance test was conducted with the sample fixed at both ends. During the test at a specified resonance frequency, acceleration level was increased by 10 G up to 60 G at a rate of 1 min. per 10 G. The short circuit current was monitored in the same way as the above two tests. The visual inspection and the electrical

Table 8. Random vibration test level.

	Freq. range (Hz)	PSD (G^2/Hz)	Overall levels (Grms)	Duration (Min)
Z	20~ 150 150~ 189 189~2000	0.2 −9 dB/OCT 0.1	14.6	1
X Y	20 20~ 35 35~ 50 50~ 126 126~ 347 347~ 520 520~2000	0.15 9 dB/OCT 0.8 −12 dB/OCT 0.02 12 dB/OCT 0.1	13.9	1

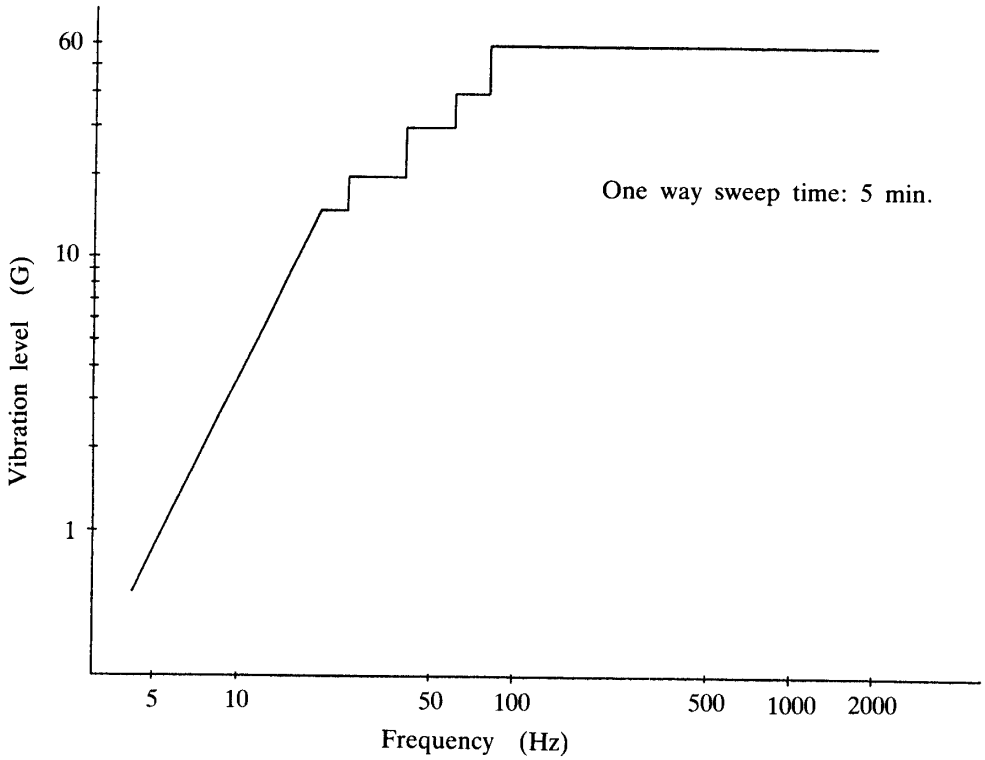

Fig. 37. Vibration level of sinusoidal vibration test.

performance tests were conducted before and after all the vibration tests, so that there was no change in the inspection and the performance test results. Besides. it was confirmed that although each intensity limit by the destruction tests was not obtained, the InP solar cells had no problem for space applications.

4.3 Ultraviolet Irradiation Test

An ultraviolet (UV) irradiation test was conducted with an irradiation facility at NEC Corporation. The test condition is shown in Table 9. Bare cells without AR coating and coverglass, cells coated with AR film without coverglass, cells coated with AR film with welding interconnector, and cells with coverglass were prepared for the test. During the test, the cell surfaces were accidentally contaminated by the oil which leaked from the diffusion pump between 528 and 1,380 ESH (Equivalent Solar Hour) fluences. So the surface reflectivity was changed and η and Isc became unusual values. The remaining factors of Voc and FF during the irradiation are shown in Fig. 38(a) and (b). The Voc was almost constant and independent of fluences, but FF was

Table 9. UV irradiation test condition.

Light source	Light intensity	Atmosphere	Temperature	Remark
Xe-Hg	6-6.5 sun	$<10^{-5}$torr	70–80°C	NEC
Xe	6–8 sun	N_2 flow	<30°C	NMC

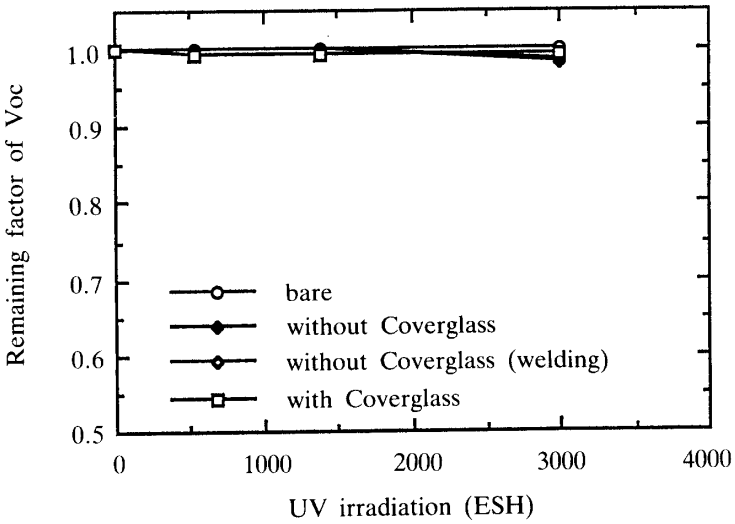

(a) Open circuit voltage

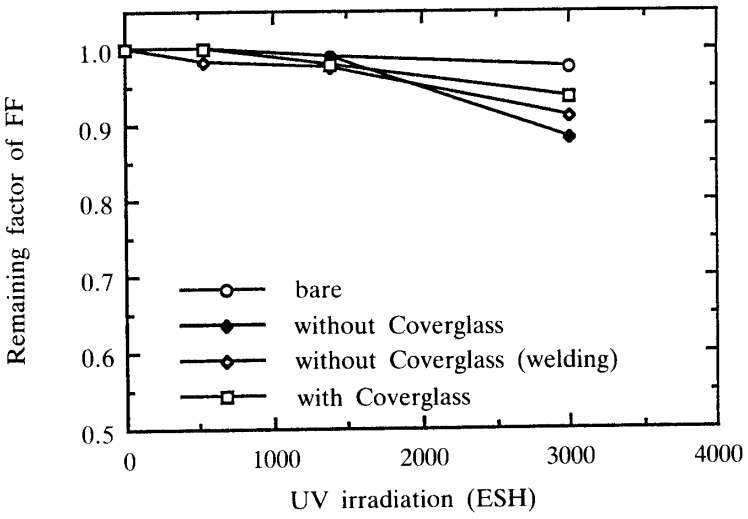

(b) Fill factor

Fig. 38. Relative cell characteristics under UV irradiation.

degraded. It should be noted that FF of the bare cells was hardly degraded. The damage of welding interconnectors was not observed. The dark I-V characteristics of the cells coated with AR film without coverglass were shown in Fig. 39.

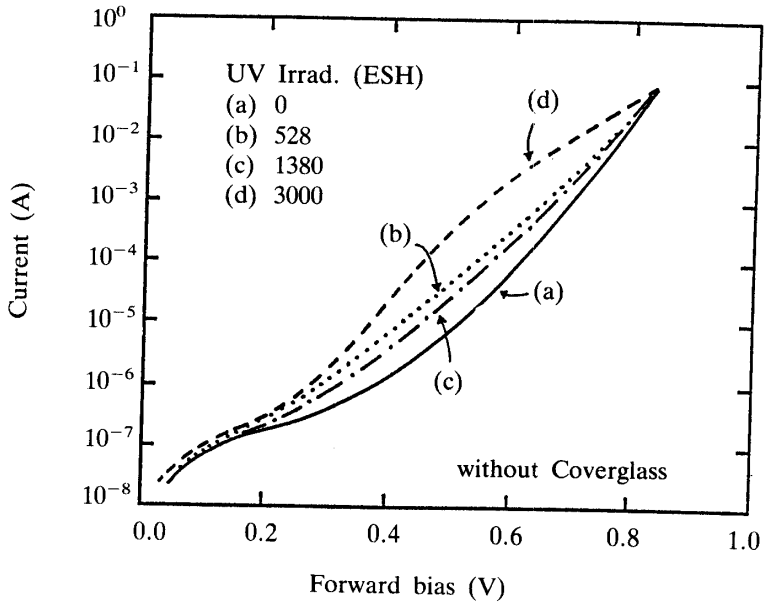

Fig. 39. Dark I-V characteristics of AR coated InP cells without coverglass.

4.4 Electron and Proton Irradiation Tests

Radiation resistance of InP solar cells to 1 MeV electrons has been studied [3] and their superior characteristics over Si and GaAs solar cells have been found as explained in section 3.4. However, the dependence of the developed cell performance on proton energy has not yet been made clear. Using those cells which were sampled in the lunar orbiter cells, we have investigated their radiation resistance to protons and electrons in wide energy range and evaluated their qualification for space applications.

4.4.1 Proton Irradiation

Proton irradiation was conducted at room temperature in the energy range from 0.015 to 15 MeV at a fluence ranging from 10^{11} to 10^{13} p/cm^2. Low energy proton (0.015 to 0.2 MeV) irradiation was performed by an ion implantation system, medium-energy proton (0.5 to 2.4 MeV) irradiation by a MV tandem accelerator, and high energy proton (3.2 to 15 MeV) irradiation by a cyclotron accelerator.

Proton damage of the cells sampled is dependent on the proton penetrating depth. Figure 40 shows the depth from the front surface where the incident protons with different energies were stopped. The Roman numerals, (i), (ii), (iii), (iv), and (v) denote n^+ layer, space charge region, deeper active region than space charge region, deeper substrate than active region, and the outside of the cell, respectively. The dependence of relative η on proton energy and fluence is shown in Fig. 41(a). The Roman numerals correspond to those of Fig. 40. At each proton fluence, there was a particular energy range at which the degradation of η was maximum. At the fluence of 10^{11} p/cm^2, the maximum degradation occurred at the proton energy of 0.1 MeV

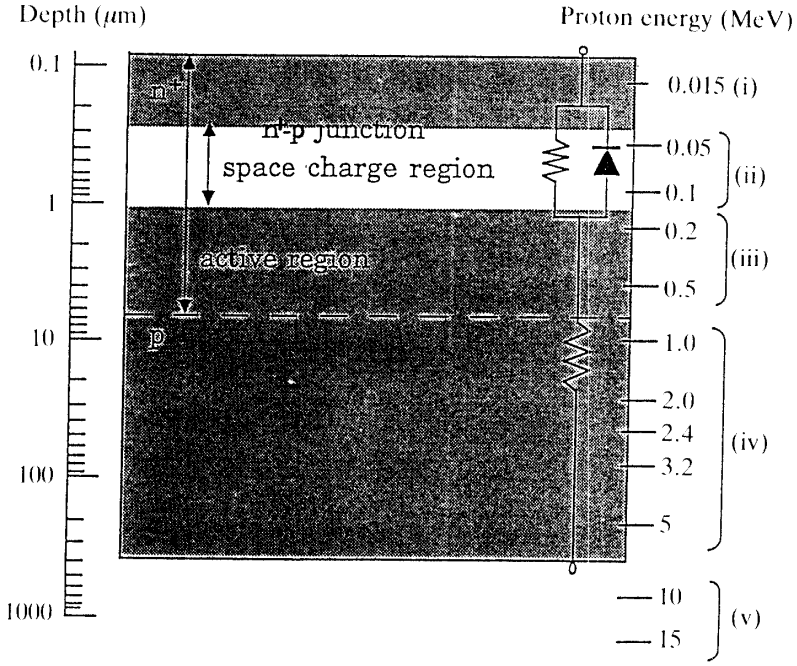

Fig. 40. Proton penetration depth in InP solar cells.

which could stop protons in the space charge region. As the fluence increased up to 10^{13} p/cm^2, the proton energy range causing the maximum degradation widened. Figure 41(b), (c), and (d) show the energy and fluence dependence of relative Voc, Isc, and FF. For fluences up to 10^{12} p/cm^2, the degradation of Voc was maximum against the protons stopped in the space charge region, whereas the degradation of Isc was very large against the protons stopped in the active region. At the fluence of 10^{13} p/cm^2, FF was mimimum for the protons stopped in the p type substrates.

The spectral response as a function of proton energy at the fluence of 10^{13} p/cm^2 is shown in Fig. 42. For lower energy protons, the blue spectral response was principally reduced, while the red response was reduced for higher energy protons. The large degradation of the spectral response was caused by the protons stopped in the active region, which corresponded with the result of Fig. 41(c). The dark I-V characteristics as a function of proton energy at 10^{12} p/cm^2 and 10^{13} p/cm^2 are shown in Figs. 43 and 44, respectively. The junction leak reaches the maximum after irradiation of the 0.1 MeV protons stopped in the space charge region, which corresponds with the result of Fig. 41(b). At the fluence of 10^{13} p/cm^2, the series resistance in the cells increases after irradiation of 1 and 5 MeV protons stopped in the p type substrates, which corresponds with the result of Fig. 41(c). We suggest that high fluence protons produce a local high resistive layer at the end of proton tracks. From the above observation, the degradation mechanism dependent on the proton penetration depth can be analyzed as follows:

1) The 0.015 MeV protons were stopped in the n layer. The blue spectral reaponse was reduced as shown in Fig. 45.
2) The 0.015–0.1 MeV protons were stopped in the space charge region. The degradation of η was large. The red spectral response was reduced for low fluence

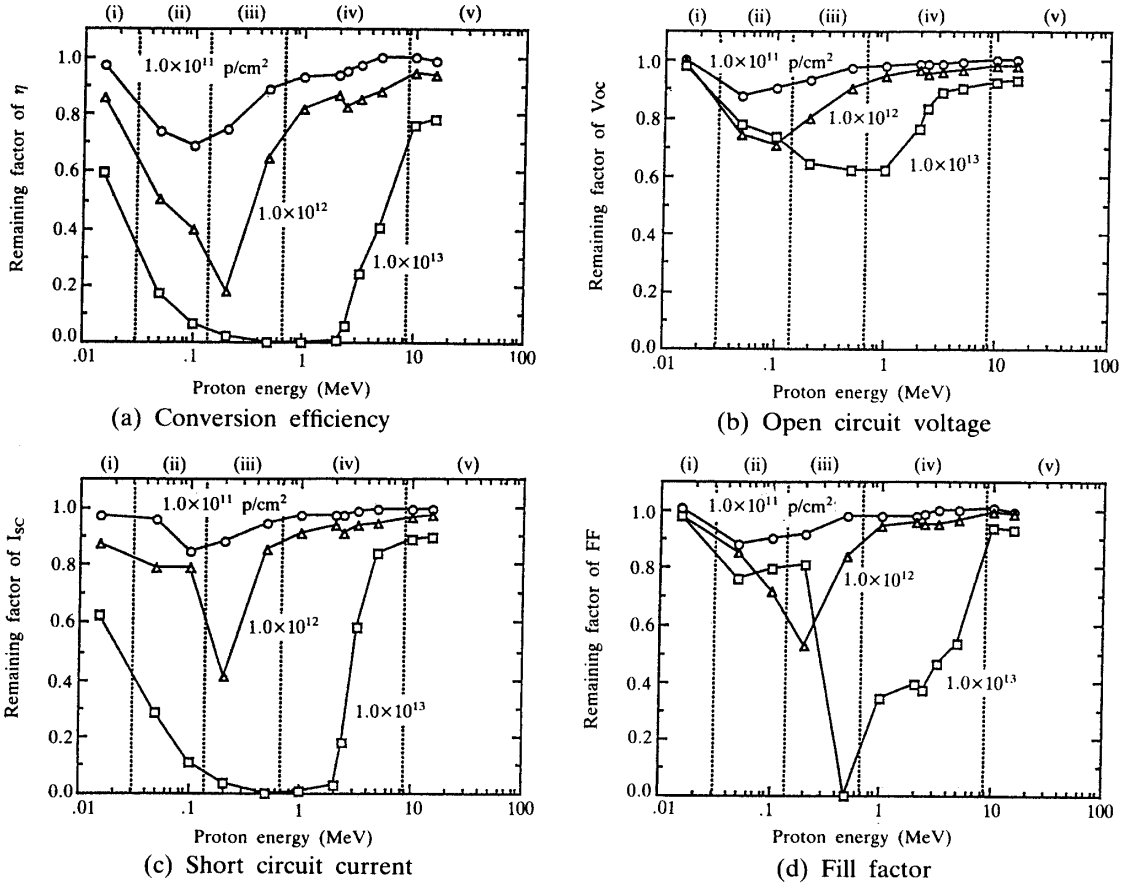

Fig. 41. Dependence of parameters of proton irradiated InP solar cells on proton energy and fluence.

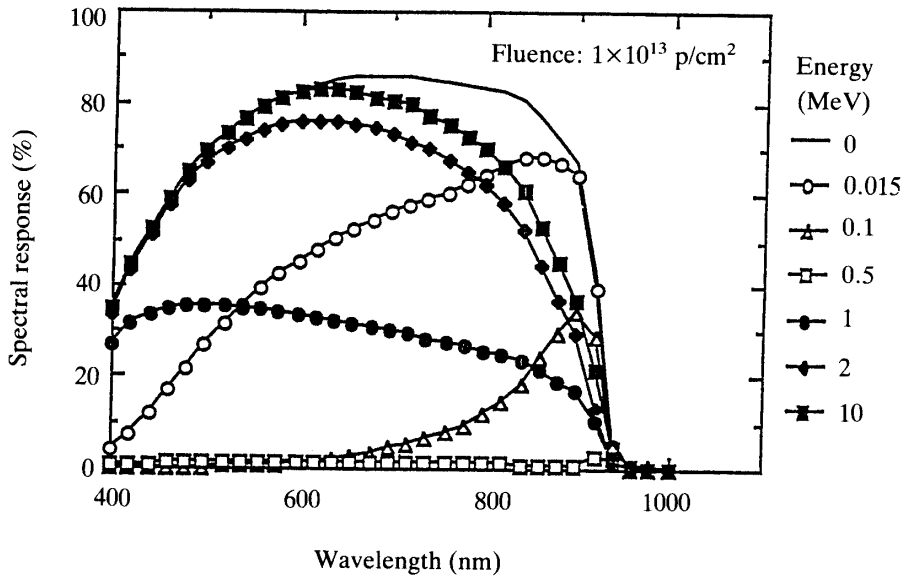

Fig. 42. Spectral response of InP solar cells considering proton energy a parameter.

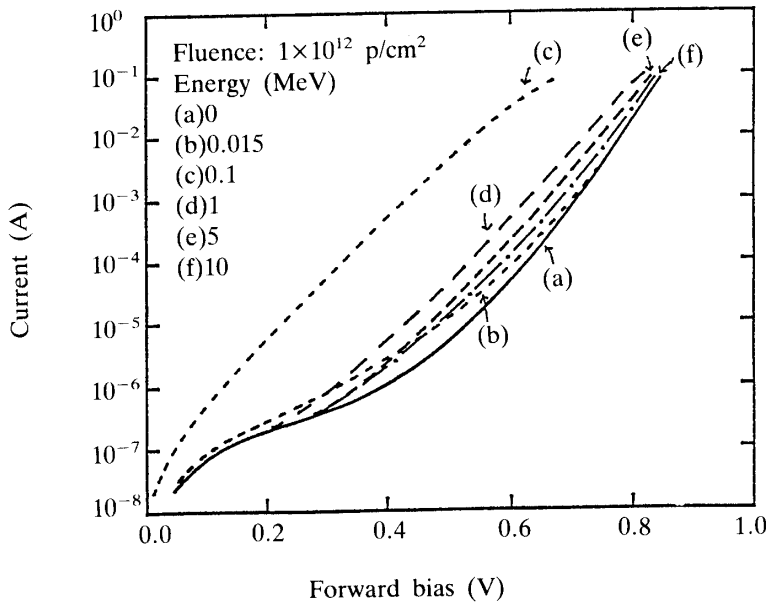

Fig. 43. Dark I-V characteristics of InP solar cells considering proton energy a parameter at fluence of 10^{12} p/cm.

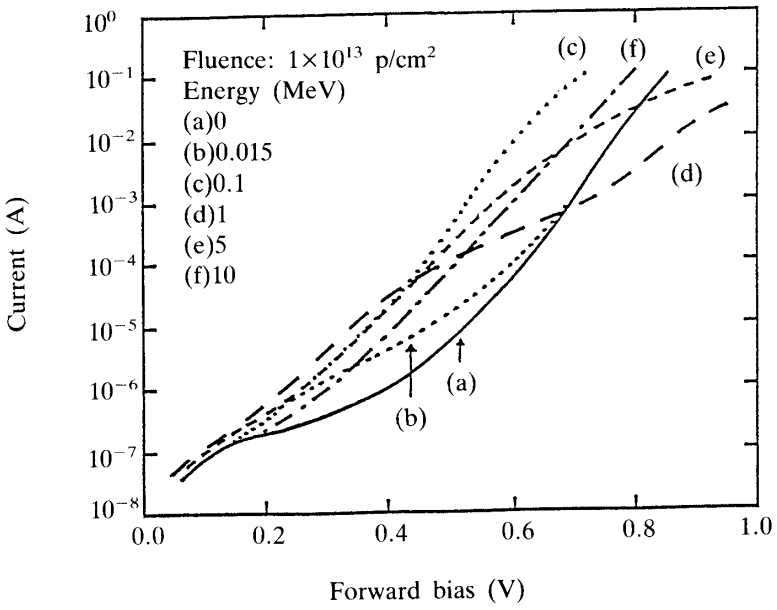

Fig. 44. Dark I-V characteristics of InP solar cells considering proton energy a parameter at fluence of 10^{13} p/cm^2.

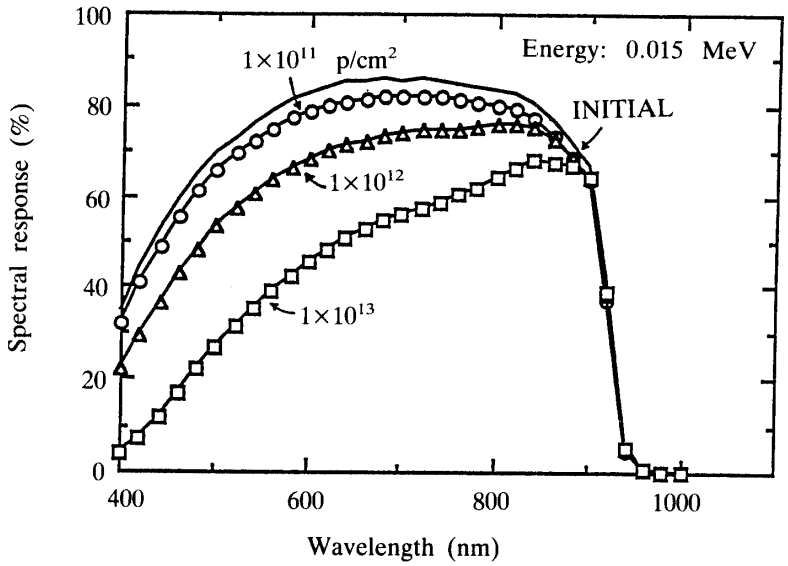

Fig. 45. Spectral response of InP solar cells considering proton fluence a parameter after 0.015 MeV proton irradiation.

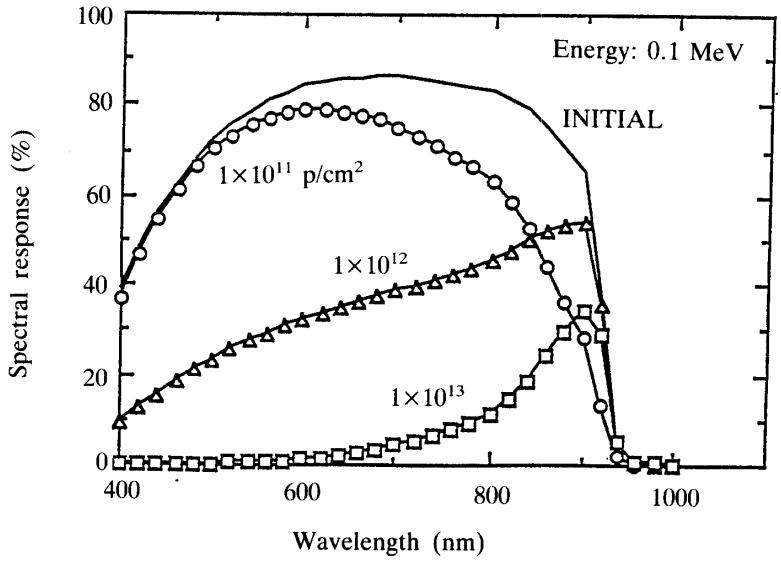

Fig. 46. Spectral response of InP solar cells considering proton fluence a parameter after 0.1 MeV proton irradiation.

protons, whereas the blue spectral response was reduced for high fluence protons as shown in Fig. 46. The high red response at high fluence levels might be explained as a result of a high resistive layer produced by protons expanding the space charge region.

3) The 0.2–0.5 MeV protons were stopped in the deeper active region than in the space charge region. The degradation of η was large. The red response was reduced as the fluence increased as shown in Fig. 47. The spectral response in entire wavelength range decreased at 10^{13} p/cm^2.

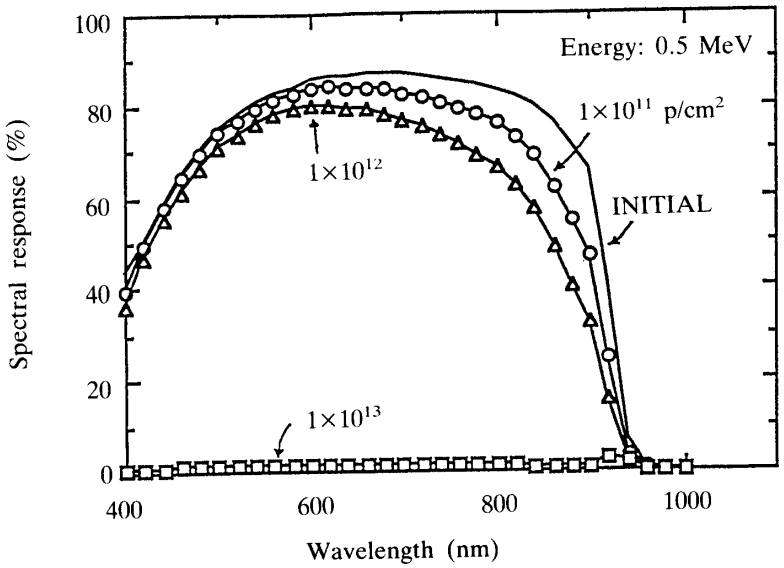

Fig. 47. Spectral response of InP solar cells considering proton fluence a parameter after 0.5 MeV proton irradiation.

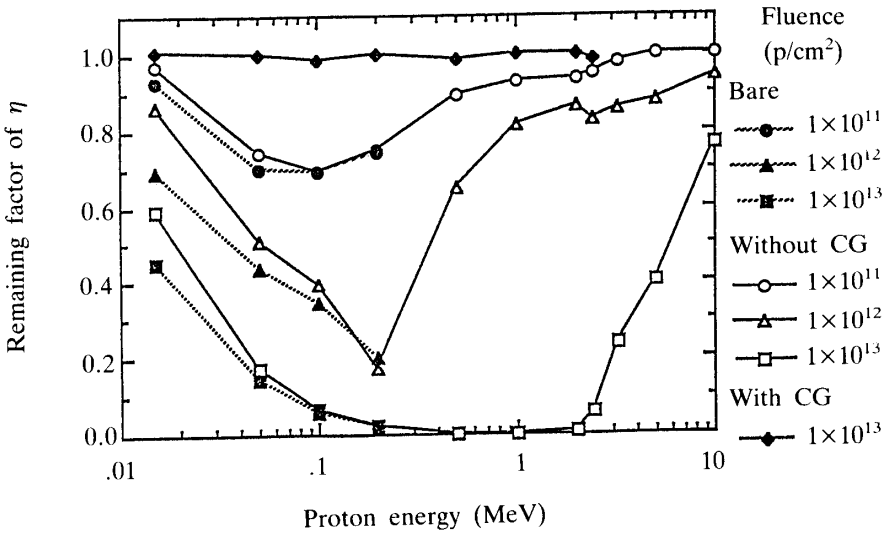

Fig. 48. Proton energy and fluence dependence of normalized efficiency for InP solar cells.

4) The 1–5 MeV protons were stopped in the deeper substrate than in the active region. The addition of the series resistance in the p type substrate reduced η. The degradation of the spectral response was small.
5) The 10–15 MeV protons penetrated through the cell. The degradation of η was small.

We have also conducted an experiment on shielding effects of coverglass and AR coating with proton irradiation. Figure 48 shows the proton energy and fluence dependence of the remaining factor of η for the InP solar cells with and without coverglass compared with bare cells, which have no AR coating and no coverglass. The cells with coverglass were irradiated with the protons up to 2.4 MeV, but no

degradation of η was observed. The damage of the cells with AR film was smaller than that of the bare cells with irradiation of the protons below 0.1 MeV. Thus the shielding effects of only 0.075 μm thick AR film were observed.

4.4.2 Electron Irradiation

Electron irradiation was performed in the energy range from 0.5 to 3 MeV and at a fluence ranging from 10^{14} to 10^{16} e/cm^2 with water cooling below 40 °C by Cockcroft-Walton's apparatus.

The electron energy and fluence dependence of the remaining factor of η for the InP solar cells with and without coverglass is shown in Fig. 49. The efficiency η was

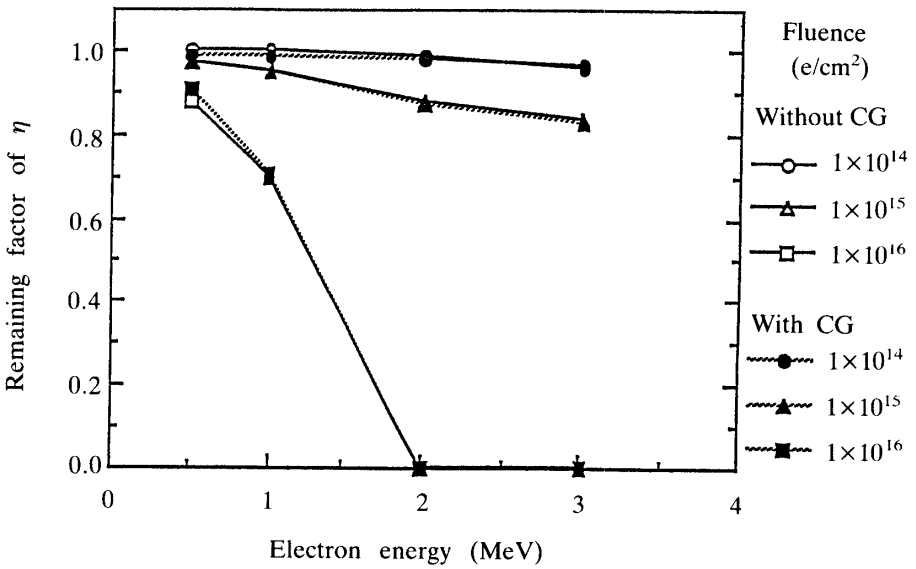

Fig. 49. Electron energy and fluence dependence of normalized efficiency for InP solar cells.

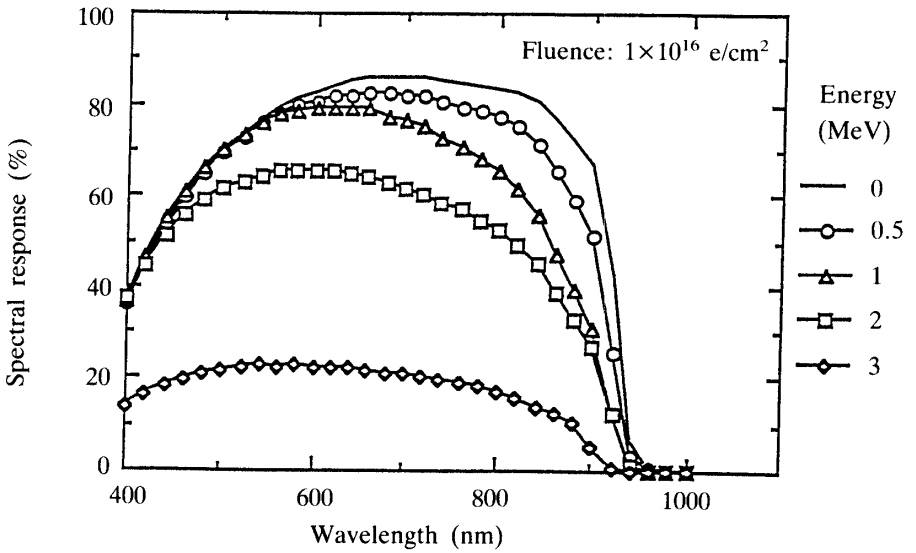

Fig. 50. Spectral response of InP solar cells considering electron energy a parameter.

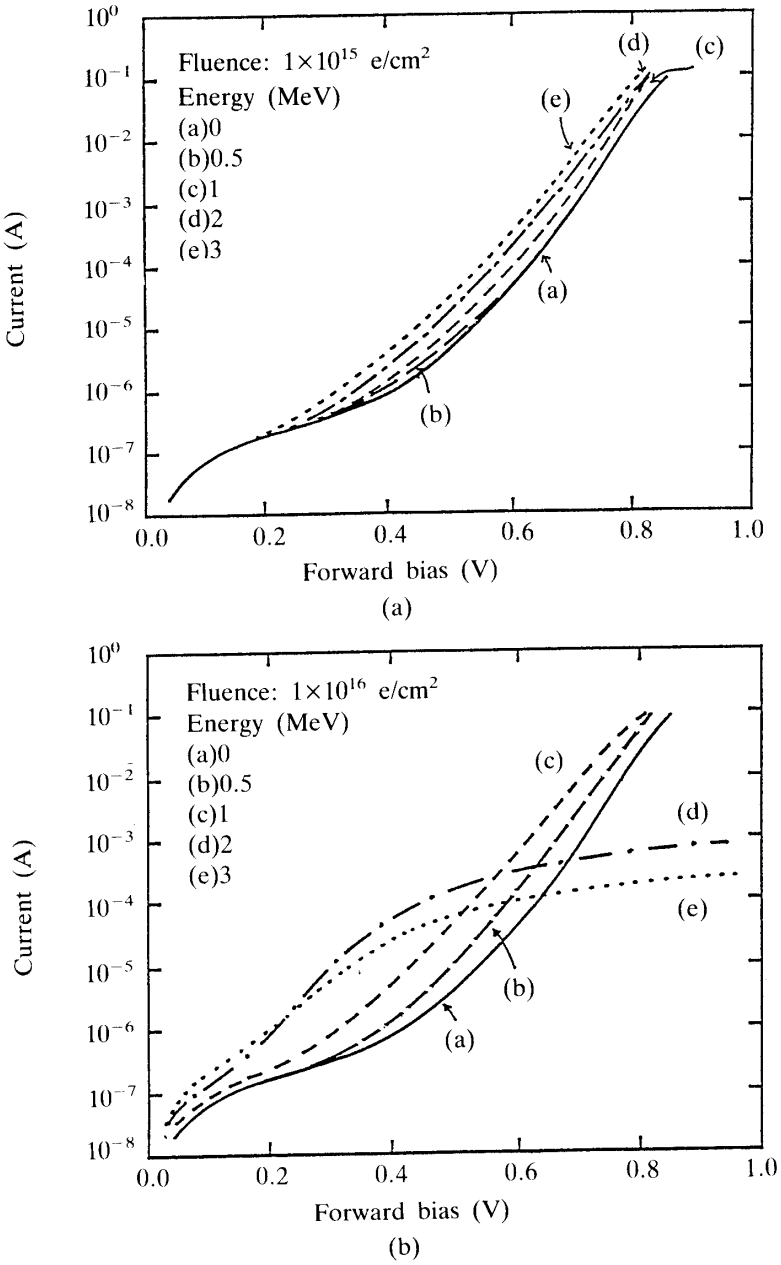

Fig. 51. Dark I-V characteristics of InP solar cells considering electorn energy a parameter.

decreased with increasing electron energy and fluence but the degradation was very small at fluences up to 10^{15} e/cm^2. Against electron irradiation, the shielding effects of 50 μm thick coverglass were not observed.

Figure 50 shows the spectral response considering electron energy a parameter at the fluence of 10^{16} e/cm^2. The red response was reduced with increasing fluence. Figure 51(a) and (b) show the dark I-V characteristics at 10^{15} and 10^{16} e/cm^2. From these results, it was found that the increase in the degradation of η against high energy electrons at the fluence of 10^{16} e/cm^2 was due mainly to a sudden increase in the series resistance in the p type substrates, as shown in Fig. 51(b).

5. Flight Experiments

In order to investigate the space radiation degradation performance, two InP solar cells without coverglass as well as two Si solar cells were mounted on the top surface of the twelfth scientific satellite "EXOS-D", which was launched in February 22, 1989 (JST) into a high altitude polar orbit for clarifying the acceleration mechanism of auroral particles.

In order to place the orbiter in orbit around the moon, the lunar orbiter that had 1,000 InP solar cells as the power source was on board the thirteenth scientific satellite "MUSES-A", which was launched on January 24, 1990 into a multiple lunar swingby orbit for demonstrating Japanese ability to place the satellite at varying distances from the earth on successive orbits [22].

5.1 SCM on board "EXOS-D"

The solar cell output degradation in orbit is considered to be due to charged particle radiation, ultraviolet radiation, thermal cycling, etc. Over the past decade, we have investigated solar cell characteristics in orbit by means of instruments on board seveal scientific satellites. As "EXOS-D" was supposed to be launched in the high altitude polar orbit according to the above objective, an instrument, SCM (Solar cell Characteristics Measurement) measuring the radiation characteristics of four solar cells was also installed on the top surface of the satellite as shown in Fig. 52.

The details of four solar cells are shown in Table 10. Two InP solar cells which were 2 cm × 2 cm in size and 400 μm in thickness and had no coverglass were mounted on a dedicated panel on the above surface to confirm the qualification for the power source on board the lunar orbiter. One Si solar cell of 50 μm in thickness was on board to evaluate the capability of the power source for the satellite "MUSES-A". The other was a 200 μm thick wraparound cell which had the possibility of large area structure due to superior weldability for future solar array applications. Fifty micron thick coverglass made of borosilicate was mounted on both Si cells. For their temperature measurement, a Pt temperature sensor was mounted on each back side of the cells.

With the instrument, the open circuit voltage and the short circuit current through the load resistor of 0.5 Ω as well as the temperature were measured. Figure 53 shows a block diagram of the SCM. Each cell output is changed into the short circuit or the open circuit condition in a current/voltage switch circuit (I/V SW). The outputs through I/V SW along with the Pt sensor outputs are sent to a telemetry subsystem via an analog switch (ANALOG SW) and a 12 bit A/D converter (ADC). The timing signal for the ANALOG SW is generated every 4 seconds. The change from the short circuit to the open circuit condition and vice versa are conducted every 576 seconds because the ANALOG SW receives 12 signal outputs from an absorptance/emittance measurement (AEM) in addition to 6 outputs from the SCM and such signal output transmission from the ADC to the telemetry subsystem is repeated 8 times on each circuit condition. The main characteristics of the SCM are shown in Table 10.

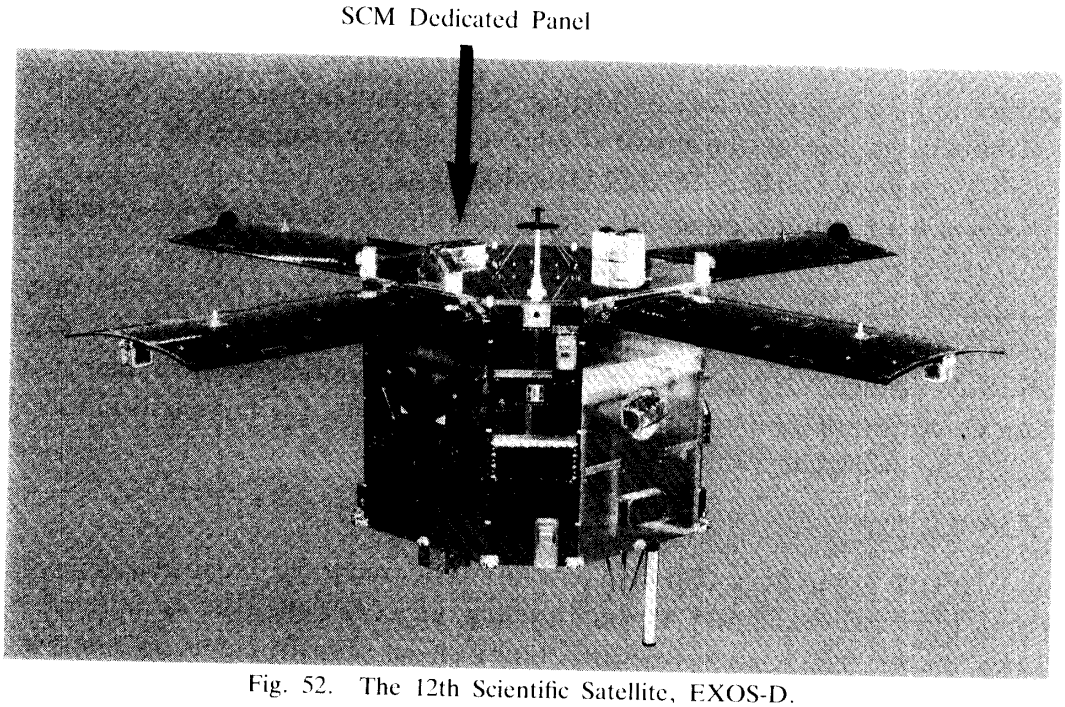

Fig. 52. The 12th Scientific Satellite, EXOS-D.

Table 10. Onboard solar cell description and SCM performance.

Channel	Solar cell description	Measured item	Sensitivity	Sampling period
SC-1	InP ·With AR coating ·20×20×0.4 mm in size ·Without coverglass	Isc	0.45 mA	·72 sec/channel ·576 sec (change period from short circuit to open circuit condition)
		Voc	0.26 mV	
SC-2	InP ·20×20×0.4 mm in size ·Without coverglass	Isc	0.45 mA	
		Voc	0.26 mV	
SC-3	Si ·BSFR CIC ·20×20×0.05 mm in size ·With coverglass	Isc	0.35 mA	
		Voc	0.20 mV	
SC-4	Si ·BSF WAC ·20×20×0.2 mm in size ·With coverglass	Isc	0.35 mA	
		Voc	0.20 mV	
TH-1	Pt sensor	Temperature for InP cells	0.05°C	·72 sec/channel
TH-2	Pt sensor	Temperature for Si cells	0.05°C	

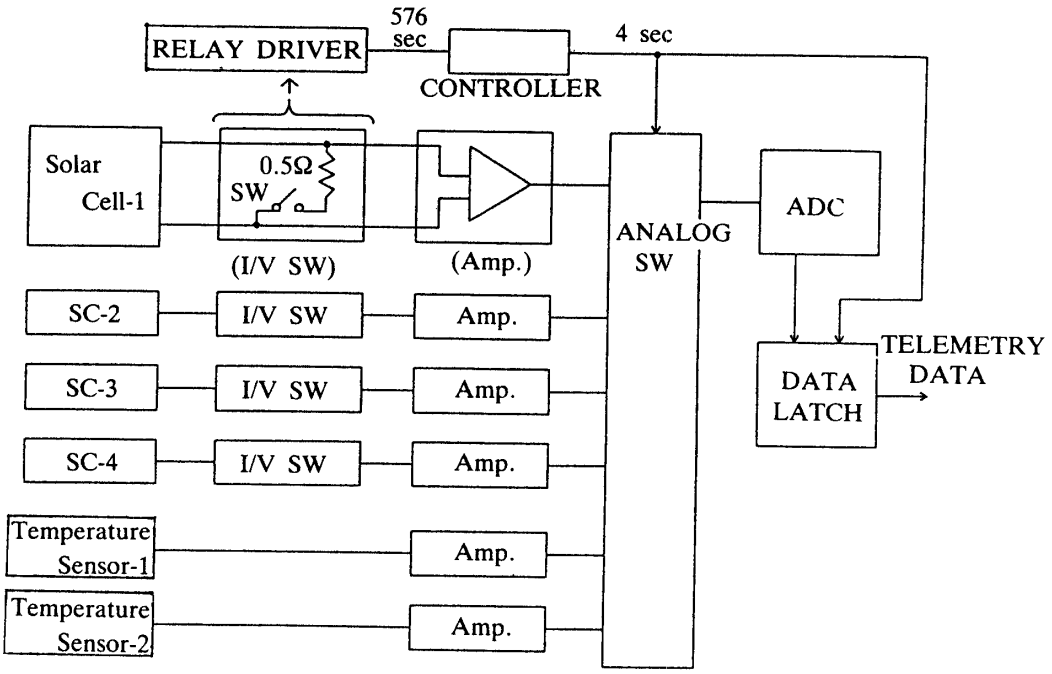

Fig. 53. Block diagram of the SCM.

5.1.1 Particle Irradiation Fluence Analysis in the Orbit for EXOS-D

According to a predicted orbit analysis of EXOS-D, Si solar cells were found to suffer from a severe output degradation due to large particle irradiation fluences since we planned to make the satellite pass the heart of the Van Allen belt. Table 11 and Figs. 54 and 55 show the proton and the electron irradiation fluences in the orbit for EXOS-D calculated from the NASA RADIATION MAP, AE8 MAX. and AP8 MAX. In order to evaluate solar cell output degradation characteristics due to these fluences, it is necessary to convert the fluences into equivalent 1 MeV electron fluences [*23*]. The result is shown in Table 12. This is based on conversion factors obtained from experimental values on Si solar cells, but cannot be applied to our InP cells as it is. As mentioned later, a new analytical model can be applied to evaluate the output degradation characteristics of the InP cells.

Table 11. Proton and electron irradiation fluences in the orbit for EXOS-D.

ENERGY (MeV)	ELECTRON FLUENCE (e/cm^2-DAY)	ENERGY (MeV)	PROTON FLUENCE (p/cm^2-DAY)
0.01	6.040×10^{12}	0.10	5.210×10^{12}
0.50	1.140×10^{11}	1.00	5.310×10^{11}
1.00	1.490×10^{10}	2.00	1.040×10^{11}
1.50	6.260×10^{9}	4.00	1.180×10^{10}
2.00	2.670×10^{9}	6.00	2.590×10^{9}
2.50	1.170×10^{9}	8.00	8.420×10^{8}
3.00	4.370×10^{8}	10.00	3.900×10^{8}
3.50	1.660×10^{8}	50.00	1.830×10^{6}
4.00	5.780×10^{7}	100.00	7.690×10^{5}
4.50	1.820×10^{7}	150.00	4.140×10^{5}
5.00	5.540×10^{6}	200.00	2.370×10^{5}
5.50	1.460×10^{6}	250.00	1.410×10^{5}
6.00	3.340×10^{5}	300.00	8.410×10^{4}
		350.00	5.060×10^{4}
		400.00	3.060×10^{4}

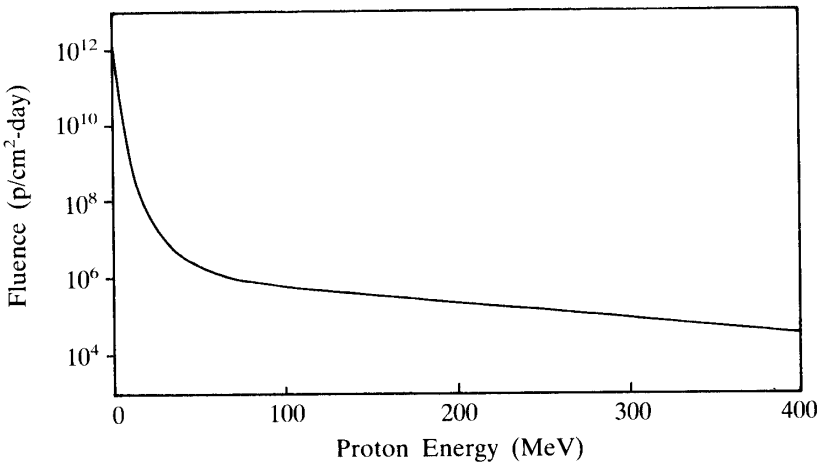

Fig. 54. Proton irradiation fluence in the orbit for EXOS-D.

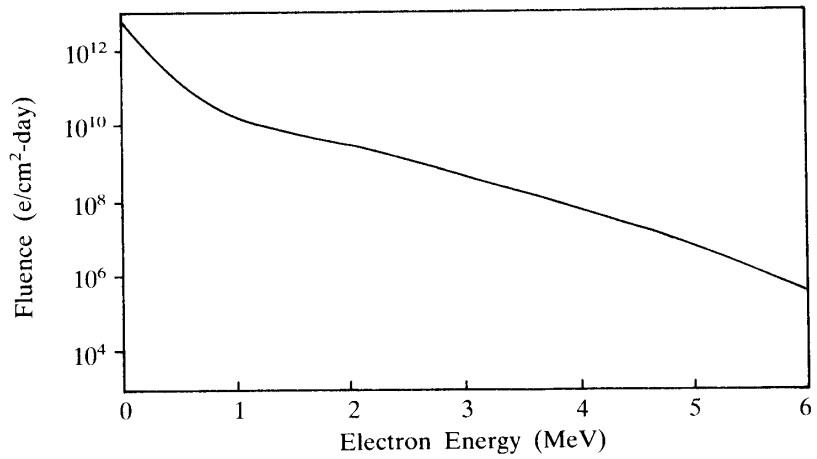

Fig. 55. Electron irradiation fluence in the orbit for EXOS-D.

Table 12. Equivalent 1 MeV electron fluences [electrons/(cm^2·day)] in the orbit for EXOS-D.

Without coverglass		With coverglass of BDX	
Isc	Voc	Isc	Voc
1.743×10^{15}	1.445×10^{16}	7.534×10^{13}	2.055×10^{14}

5.1.2 Flight Result of SCM

The satellite "EXOS-D" was launched into an orbit of the inclination of 75°, the apogee height of 10,500 km, and the perigee height of 274 km. The SCM started the measurement of all the cells and their temperature on the 2nd day after the launch and its function was confirmed to be normal. Analytical results obtained from flight data since the 2nd day are shown in Figs. 56 through 59. These results are normalized on

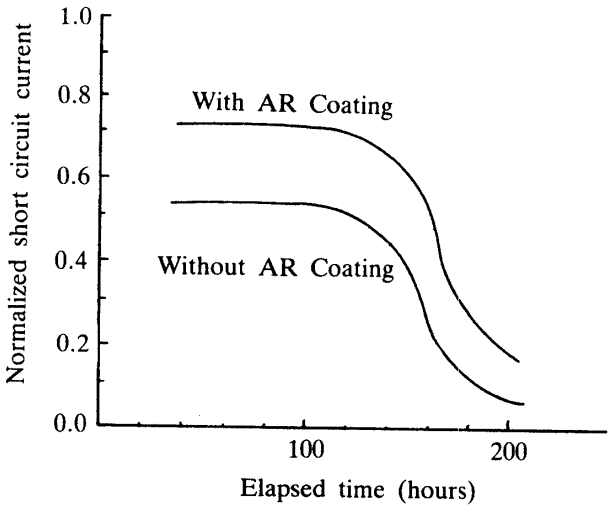

Fig. 56. Normalized flight data of Isc for InP solar cells.

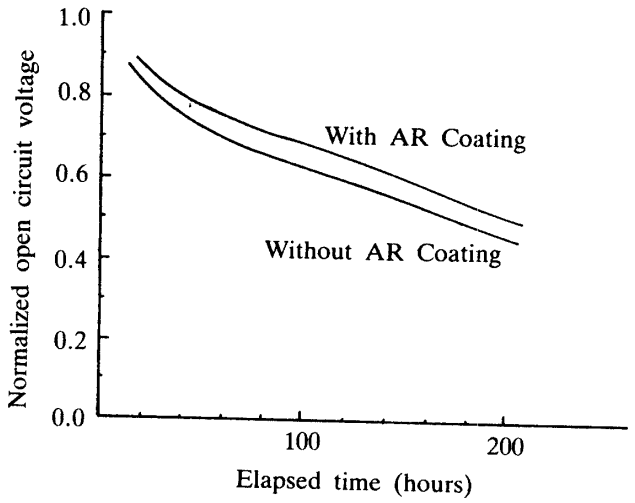

Fig. 57. Normalized flight data of Voc for InP solar cells.

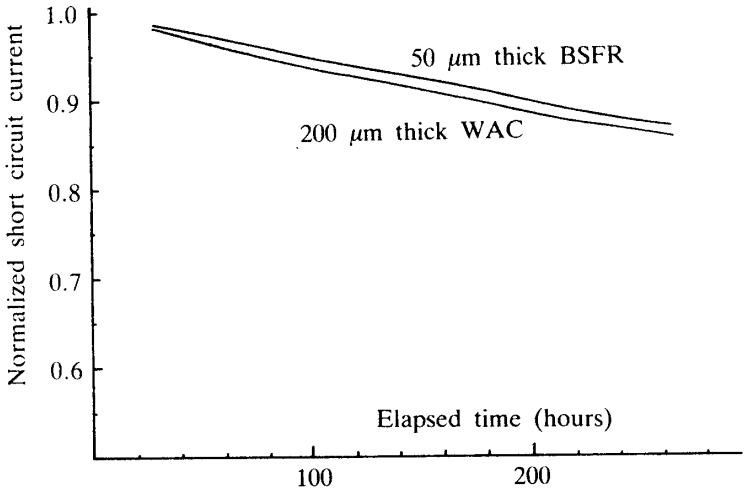

Fig. 58. Normalized flight data of Isc for Si solar cells.

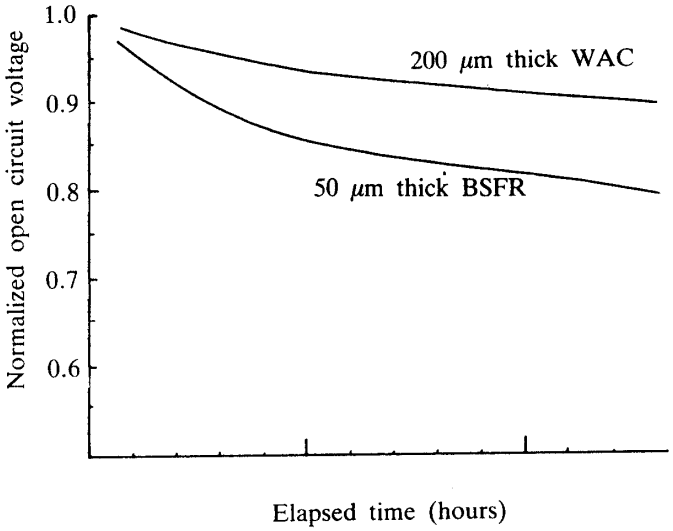

Fig. 59. Normalized flight data of Voc for Si solar cells.

the condition of one solar constant of 135.3 mW/cm^2, the cell temperature of 28 °C, and normal incidence. The output degradation of the InP cells without coverglass in Figs. 56 and 57 seems to be much larger than that of the electron irradiation test on the ground. This suggests that a new analytical model is required to explain the output degradation characteristics of the InP cells. In contrast with this, the output degradation of the Si cells with coverglass in Figs. 58 and 59 is as almost predicted.

5.2 LO on board "MUSES-A"

In "MUSES-A", the LO was on board to place it in orbit around the moon as the first trial for lunar exploration in Japan when "MUSES-A" closed to the moon about one month after the launch. One thousand InP solar cells of 1 cm × 2 cm in size with coverglass made of borosilicate glass, BDX of thickness of 50 μm were mounted on the polyhedral structure surface of the LO as shown in Fig. 60. This solar array can supply about 10 W to onboard electronics such as a data processing unit (DPU), an S

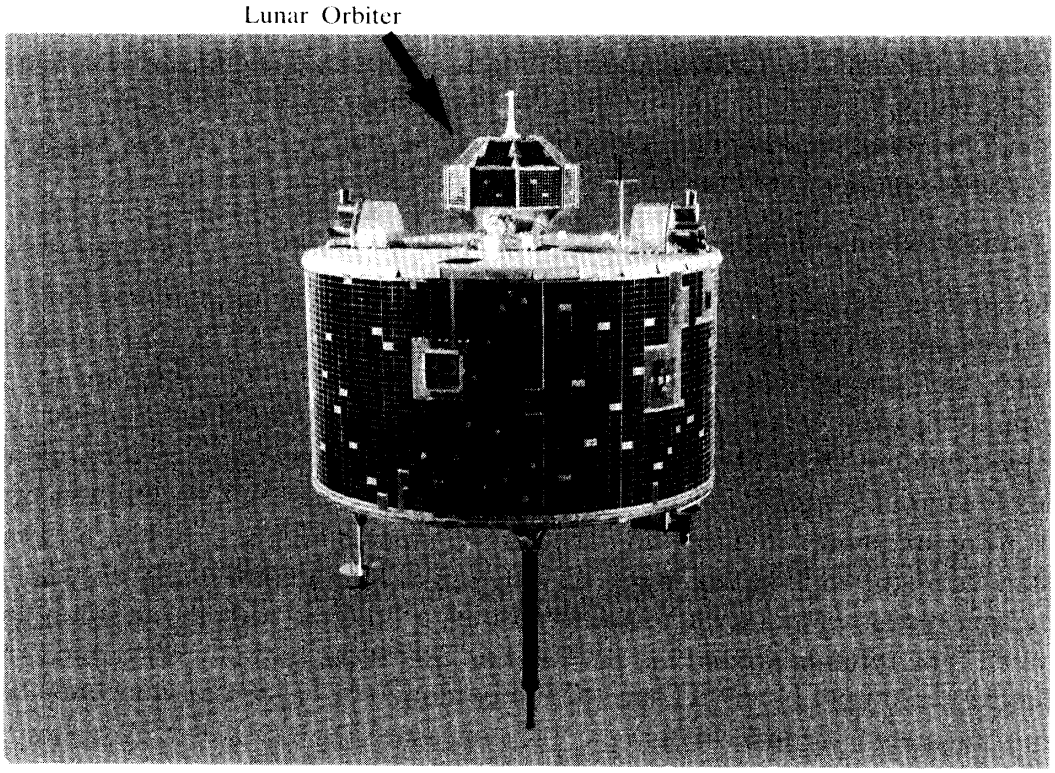

Fig. 60. The 13th scientific satellite, MUSES-A.

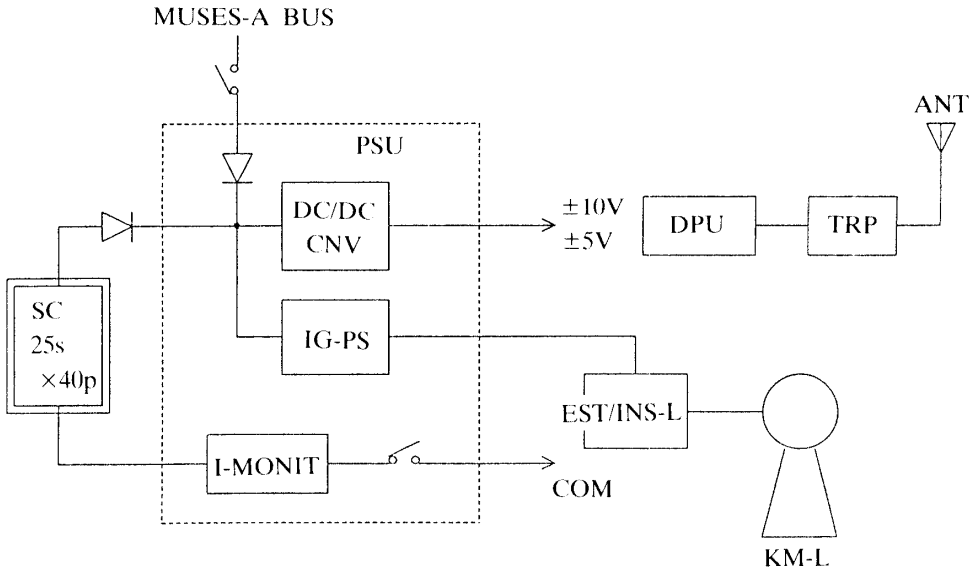

Fig. 61. Block diagram of LO.

band transponder (TRP), an electronic sequential timer/environmental instrument (EST/INS-L), and so on through a DC/DC converter (DC/DC CNV), as shown in a block diagram in Fig. 61. By transmitting commands from the ground, the power subsystem for the satellite can supply power required to the orbiter or stop supplying power.

The solar array for the LO consists of cell assemblies, blocking diodes, substrates, and wire harnesses. The cell assemblies comprise 25 series and 40 parallel connected InP cells, being mounted on the 16 faces of a 24 polyhedral body. The substrates use 2 plies of Kevlar fiber/epoxy prepreg (0.2 mm thick) as a face sheet and the 4 mm thick honeycomb sandwich structure with Al 1/8–5052–.001p as their core.

5.2.1 Flight Result of LO

The satellite "MUSES-A" was launched into an orbit of the inclination of 30.6°, the apogee height of 286,390.9 km, and the perigee height of 216.85 km. During the swingby orbit phase before the separation of the LO, the LO performance was sometimes checked by the commands which could connect or disconnect the solar array with the DC/DC CNV. In the meantime, the TRP transmitted the performance data to the ground station, UDSC (Usuda Deep Space Center). Check results of the solar array are shown in Table 13. The array output power is found to be almost constant as predicted as shown in Fig. 62 which gives an analytical result of solar array generation power, although it practically varies a little bit with the rotation angle because of the rotation around the satellite spin axis at the spin rate of 20 rpm. Thus, no decrease in output power is concluded to be caused by charged particle radiation.

Unfortunately, late in February the TRP on board the LO failed. Afterward we could not communicate with the LO directly. However, On March 19, 1990 with a schmidt camera, Kiso Observatory (University of Tokyo) confirmed that the orbiter separated from "MUSES-A" as planned. From a prototype model simulation, we probably infer that the failure is due to a turn-on transient output of the DC/DC CNV in the case of the above check operation by the commands.

Table 13. Flight data of solar array on LO. In the meantime, the θs ranged from 87° to 93°.

TIME (UT)	SC-V	SC-I	TEMP-1	TEMP-2
1990/ 1/24 22:23	19.78 V	0.394 A	−2.6 °C	9.2 °C
1/28 01:33	19.78	0.394	−2.6	9.2
2/ 3 01:22	19.98	0.394	−4.1	7.7
2/20 22:37	19.58	0.353	−7.0	6.2
2/21 22:18	19.98	0.353	−7.0	6.2
23:17	20.08	0.341	−7.0	7.7
3/15 00:48	19.78	0.359	+1.8	12.2
3/18 17:36	19.98	0.347	−2.6	9.2

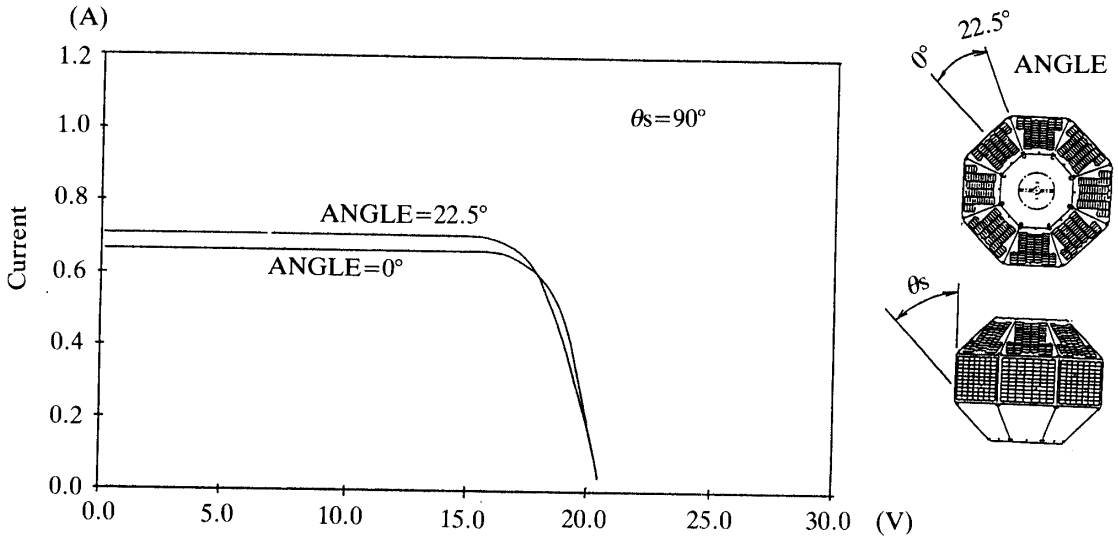

Fig. 62. Predicted I-V characteristics of solar array for LO. The θs is an angle between the sun and the spin axis of LO.

6. Discussion

According to the proton and electron irradiation effects on our InP solar cells described in section 4.4, the flight data of the onboard InP cells in the "EXOS-D" orbit have been analyzed [*24, 25*]. However, consequently proton irradiation effects on the InP cells have only been considered since no degradation of the InP cells due to electrons in the orbit has been observed.

6.1 Analytical Model

In general, radiation-induced defects in the solar cell active region cause the decrease in the minority carrier diffusion length L and thus the short circuit current density J_{sc} and the open circuit voltage V_{oc} for the solar cells are expected to be decreased with the proton or electron fluence ϕ as follows:

$$\Delta(1/J_{sc}^2)=1/J_{sc\phi}^2-1/J_{sc0}^2\propto\Delta(1/L^2)=K_L\phi, \tag{13}$$

$$\Delta(1/[\exp(V_{oc})]^2)=1/[\exp(V_{oc\phi})]^2-1/[\exp(V_{oc0})]^2 \propto\Delta(1/J_{sc}^2), \tag{14}$$

where suffixes 0 and ϕ show before and after irradiation, and K_L is the damage coefficient for the diffusion length. In the following paragraphs, the proton and electron irradiation effects on the InP solar cells have been examined experimentally based on the above equations.

6.1.1 Analytical Model for Proton Irradiation

Figure 63 shows changes in inverse square of the short circuit current density of InP cells, $\Delta(1/J_{sc}^2)$ as a function of proton fluence and energy. The proton fluence dependence of J_{sc} is found to be expressed by

$$\Delta(1/J_{sc}^2)=A\phi^{0.7}+B\phi^5, \tag{15}$$

where A and B are coefficients. The first term of Eq. (15) indicates the degradation due to minority carrier diffusion length decrease caused by recombination center generation with proton irradiation and the 0.7 power dependence is thougth to be due to nonuniform defect distribution with proton irradiation. The second term is associated with series resistance increase due to base layer carrier concentration reduction caused by majority carrier trapping center generation with proton irradiation.

Figure 64 shows the proton energy dependences of the coefficients A and B, which have been determined based on the proton irradiation results for the InP solar cells. Changes in the coefficients A and B as a function of proton energy, Ep MeV are approximated by

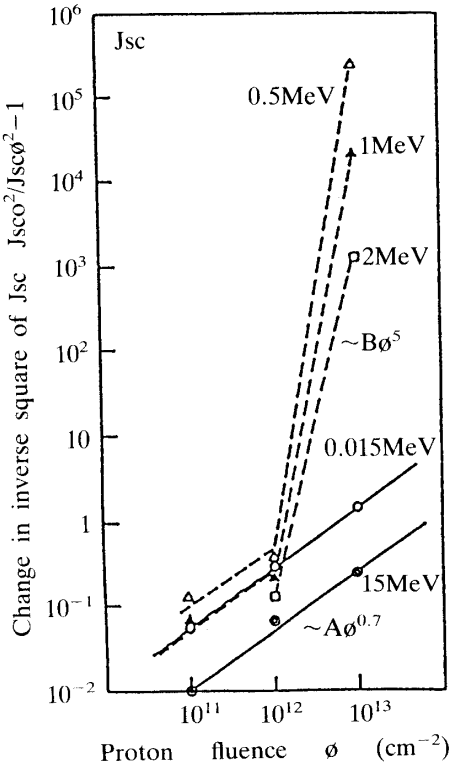

Fig. 63. Changes in inverse square of short circuit current density of InP solar cells as a function of proton fluence and energy.

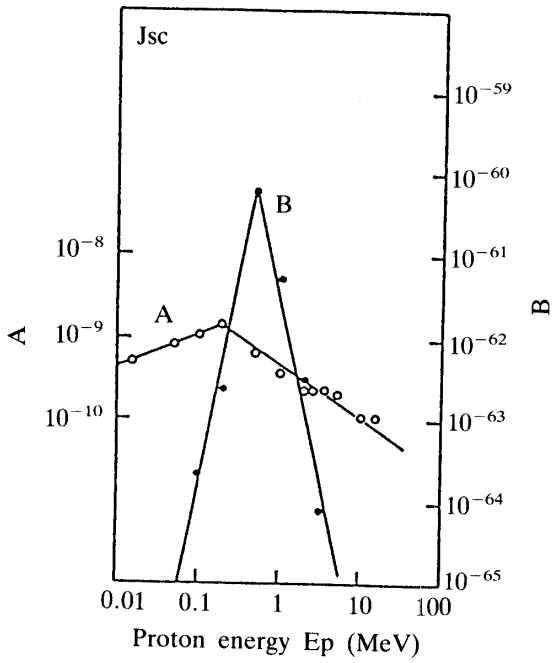

Fig. 64. Proton energy dependence of coefficients A and B, determined based on proton irradiation results for InP solar cells.

$$A=2.8\times10^{-9}Ep^{0.4}, \quad Ep\leq0.2MeV, \tag{16}$$

$$A=5\times10^{-10}Ep^{-0.67}, \quad Ep>0.2MeV, \tag{17}$$

$$B=2.14\times10^{-59}Ep^{5.1}, \quad Ep\leq0.5MeV, \tag{18}$$

$$B=2.58\times10^{-62}Ep^{-4.6}, \quad Ep>0.5MeV. \tag{19}$$

Moreover, as shown in Fig. 65, the open circuit voltage degradation due to proton irradiation is found to be given by

$$\Delta(1/[\exp(V_{oc})]^2)=C\phi^{0.6}, \tag{20}$$

where C is a coefficient. The 0.6 power dependence in Eq. (20) is thought to be due to nonuniform defect distribution with proton irradiation.

Figure 66 shows the proton energy dependences of the coefficient C, which has been determined based on the proton irradiation effects of the InP solar cells. Changes in the coefficient C as a function of proton energy Ep MeV are approximated by

$$4.9\times10^{-7}Ep^{2.25}, \quad Ep\leq0.05MeV, \tag{21}$$

$$2\times10^{-9}Ep^{0.42}, \quad 0.05<Ep\leq0.2MeV, \tag{22}$$

$$C=1\times10^{-9}, \quad 0.2<Ep\leq0.5MeV, \tag{23}$$

$$4.7\times10^{-10}Ep^{-1}, \quad 0.5<Ep\leq1MeV, \tag{24}$$

$$4.4\times10^{-10}Ep^{-0.4}, \quad Ep>1MeV. \tag{25}$$

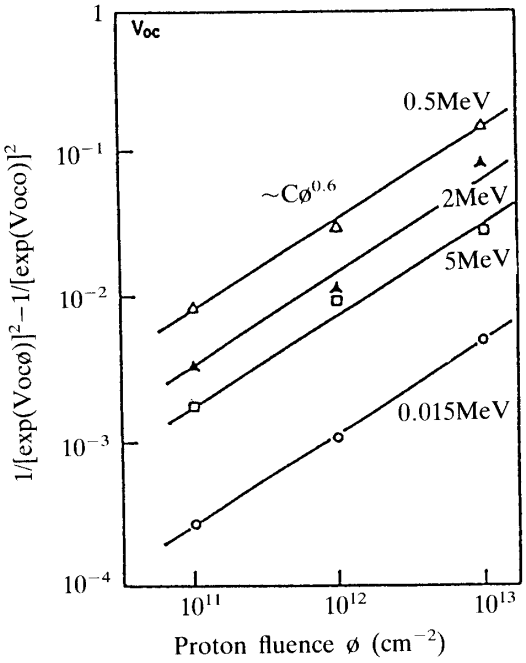

Fig. 65. Changes in open circuit voltage of InP solar cells as a function of proton fluence and energy.

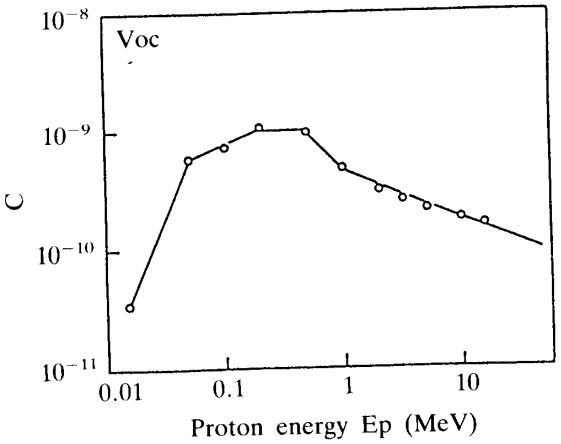

Fig. 66. Proton energy dependence of coefficient C, determined based on proton irradiation results for InP solar cells.

6.1.2 Analytical Model for Electron Irradiation

Figure 67 shows the electron and proton energy dependences of damage coefficients calibrated by the 1 MeV electron irradiation damage for InP solar cells.

Although experimental results are not shown in figures, the following equations for the electron fluence dependence of InP solar cell properties are derived from the experimental results. The electron fluence dependence of J_{sc} is found to be expressed by

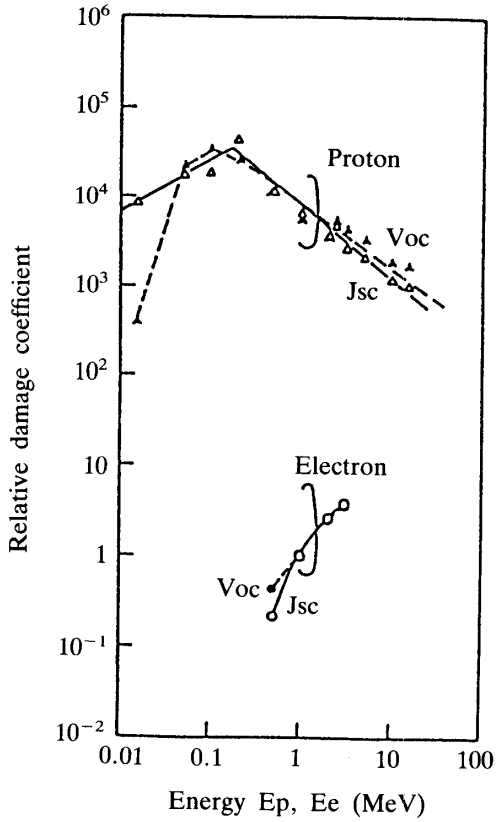

Fig. 67. Electron and proton energy dependences of damage coefficients, calibrated by 1 MeV electron irradiation damage, for InP solar cells.

$$\Delta(1/J_{sc}^2)=A\phi+B\phi^5, \tag{26}$$

where A and B are coefficients and ϕ is the electron fluence. As described above, the first term of Eq. (26) indicates the degradation due to minority carrier diffusion length decrease caused by recombination center generation with electron irradiation. The mechanism is confirmed by the linear relationship between $\Delta(1/J_{sc}^2)$ and electron fluence, which shows uniform defect distribution due to electron irradiation. The second term is associated with series resistance reduction caused by majority carrier trapping center generation with electron irradiation. Changes in the coefficients A and B as a function of electron energy, Ee MeV are approximated by

$$A=3.8\times10^{-17}Ee^{1.9}, \tag{27}$$

$$B=2.2\times10^{-81}Ee^{9}. \tag{28}$$

The open circuit voltage degradation due to electron irradiation is found to be given by

$$\Delta(1/[\exp(V_{oc})]^2)=C\phi, \tag{29}$$

where C shows a coefficient. As described above, Eq. (29) indicates the degradation due to minority carrier diffusion length decrease caused by recombination center generation with electron irradiation. This is confirmed by the linear relationship between electron fluence and $\Delta(1/[\exp(V_{oc})]^2)$, which shows uniform defect distribution due to electron irradiation. Changes in the coefficient C as a function of electron energy Ee MeV is approximated by

$$C=4.4\times10^{-18}Ee^{1.33} \tag{30}$$

6.2 Analysis for Flight Data of InP Solar Cells on board EXOS-D

The flight data of the InP solar cells in the EXOS-D orbit have been analyzed based on the analytical model described above and the proton fluence data in the orbit in Fig. 54. Actually, the energy dependence of proton fluences has been expressed by dividing the range of 0 to 10 MeV into 20 parts as shown in Fig. 68. Proton irradiation damages to the InP solar cells have also been expressed by Eqs. (15) to (25).

Figure 69 shows comparison between analytical results and the flight data for InP cell properties. Good agreement between them shows the validity of the analytical model. Although the InP cells without coverglass show severe short circuit current reduction after about 1 week when the total irradiation flux corresponds to the equivalent 1 MeV electron fluence of 2×10^{16} cm^{-2}, radiation resistance of the InP

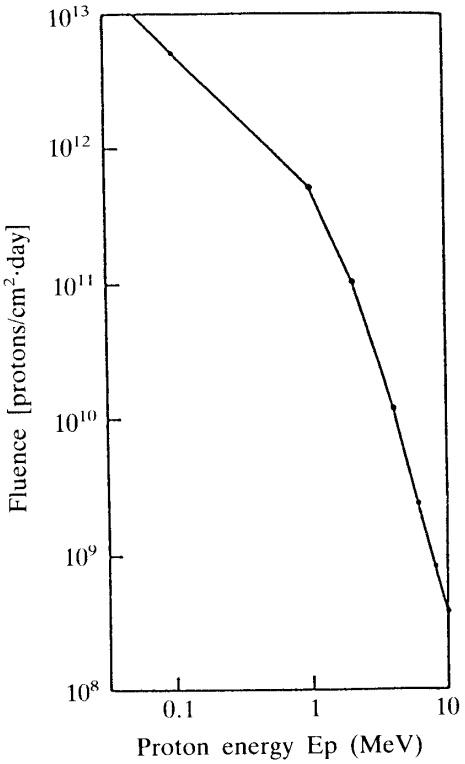

Fig. 68. Proton irradiation fluences divided into 20 parts in the range of 0–10 MeV in the orbit for EXOS-D.

cells is found to be improved with 50 μm thick coverglass as shown in this figure and to be much better than that of Si and GaAs cells. Moreover, this resistance is also found to be improved with high carrier concentration substrates because the short circuit current reduction due to proton irradiation is mainly caused by the reduction in the carrier concentration in InP substrates.

Our InP solar cells are concluded to be applicable to space solar cells in severe radiation environments such as EXOS-D orbit environments by using thin coverglass.

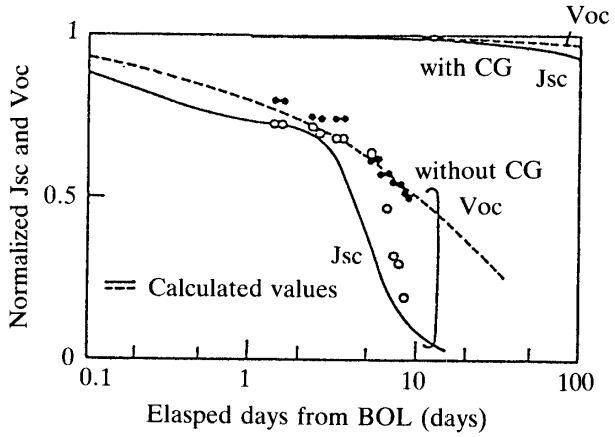

Fig. 69. Comparison between analytical results and flight data.

7. Conclusions

We have developed high-efficiency homojunction 1 cm × 2 cm InP space solar cells by diffusing In_2S_3 into p type InP substrates and investigated their fundamental characteristics such as electrical characteristics, thermal properties, and mechanical characteristics.

Since it is important for space solar cells to be resistant to space radiation, we have studied the radiation resistant mechanism of InP cells fabricated at NTT Opto-electronics Laboratories over the last several years and found superior properties such as room temperature annealing and minority carrier injection enhanced annealing phenomena for radiation-induced defects in InP crystals with 1 MeV electron irradiation. We have also found that InP cells are superior to Si and GaAs cells in radiation resistance. Superior rediation resistance of InP cells is due to the energy band structure in comparison with Si cells and due to the lower defect introduction rate in comparison with GaAs cells.

In order to evaluate the developed InP cells in the simulated space environment and to give them the qualification for space applications, various tests such as vibration, thermal cycling, ultraviolet ray, and proton and electron irradiation tests were conducted on the ground. The proton irradiation test energy and fluences ranged from 0.015 to 15 MeV and from 10^{11} to 10^{13} p/cm^2, respectively. The electron irradiation test energy and fluences ranged from 0.5 to 3 MeV and from 10^{14} to 10^{16} e/cm^2,

respectively. As a result, we have confirmed that the series resistance in the cells increases owing to the decrease in the majority carrier concentration at higher fluences even with proton irradiation.

The developed InP solar cells were mounted on the scientific satellite "EXOS-D" encountering severe radiation environments as the radiation degradation characteristic instrument and on the lunar orbiter on board the scientific satellite "MUSES-A" as the power source for the lunar orbiter. We succeeded in working those solar cells in orbit. The large decreases in the short circuit current and in the open circuit voltage for the InP cells without coverglass on board "EXOS-D" turned out to be due to lower energy proton irradiation with our new analytical model. However, it has been confirmed that no degradation of the InP cells occurs by using thin coverglass of 50 μm in thickness.

Output power of the solar array for the lunar orbiter was constant as predicted till the separation from "MUSES-A" to place the orbiter in orbit around the moon.

From the above description, we conclude that the InP solar cells are applicable to space solar cells under severe radiation environments in orbit.

We are considering more long-term evaluation of the InP cells with UV irradiation as soon as possible, although the reliable cell characteristics have been obtained up to 528 ESH fluences. For further improvement in efficiency, weight, and cost in our InP solar cells, it is essential to develop thin film InP cells fabricated on Si substrates together with more positive introduction of the back surface field structure.

Acknowledgments

The authors wish to express their sincere thanks to Prof. T. Nishimura, Prof. K. Uesugi, and Assoc. Prof. M. Tajima for many beneficial advices and discussions. The authors are also grateful to the related personnel of the ISAS for the data acquisition concerning the two scientific satellites and the lunar orbiter.

References

[1] Yamaguchi M., Yamamoto A., Itoh Y., and Uemura C.: "22 % efficient and high radiation-resistant InP solar cells", Proc. 2nd International Photovoltaic Science and Engineering Conference, Beijing, China, pp. 573–578 (1986).

[2] Yamaguchi M., Uemura C., and Yamamoto A.: "Radiation damage in InP single crystals and solar cells", J. Appl. Phys., 55, 6, pp. 1429–1436 (1984).

[3] Yamaguchi M., Uemura C., Yamamoto A., and Shibukawa A.: "Electron irradiation damage in radiation-resistant InP solar cells", Jpn. J. Appl. Phys., 23, 3, pp. 302–307 (1984).

[4] Yamaguchi M., Itoh Y., and Ando K.: "Room-temperature annealing of radiation-induced defects in InP solar cells", Appl. Phys. Lett., 45, 11, pp. 1206–1208 (1984).

[5] Yamaguchi M., Ando K., Yamamoto A., and Uemura C.: "Minority-carrier injection annealing of electron irradiation-induced defects in InP solar cells", Appl. Phys. Lett., 44, 4, pp. 432–434 (1984).

[6] Yamaguchi M., Hayashi T., Ushirokawa A., Takahashi K., Kohbata M., Hashimoto M., Okazaki H., Takamoto T., Ura M., Ohmori M., Ikegami S., Arai H., and Orii T.: "First space flight of InP solar cells", Proc. 21st IEEE Photovoltaic Specialists Conference, Kissimmee, U.S.A., pp. 1198–1202 (1990).

[7] Takamoto T., Okazaki H., Takamura H., Ura M., Ohmori M., Yamaguchi M., Ikegami S., Arai H., Hayashi T., Ushirokawa A., Takahashi K., Kohbata M., and Ohnishi A.: "Indium phosphide solar

cells for space applications, Proc. 5th International Photovoltaic Science and Engineering Conference, Kyoto, Japan, pp. 547–550 (1990).

[8] Bailey S.G., Weinberg I., and Flood D.J.: "Enhanced EOS photovoltaic power system capability with InP solar cells", Proc. European Space Power Conference, Florence, Italy, esa SP-320, pp. 641–645 (1991).

[9] Okazaki H., Takamoto T., Takamura H., Kamei T., Ura M., Yamamoto A., and Yamaguchi M.: "Production of indium phosphide solar cells for space power generation", Proc. 20th IEEE Photovoltaic Specialists Conference, Las Vagas, U.S.A., pp. 886–892 (1988).

[10] Goradia G., Geier J.V., and Weinberg I.: "Modelling and design of high efficiency radiation tolerant indium phosphide solar cells", Proc. 19th IEEE Photovoltaic Specialists Conference, New Orleans, U.S.A., pp. 937–943 (1987).

[11] Hayashi T., Ushirokawa A., Ohnishi A., Masumoto Y., Arai H., Hagino S., Wada M., Yamamoto S., and Onoda T.: "Borosilicate cover glass for solar cell of EXOS-D", Proc. 19th IEEE Photovoltaic Specialists Conference, New Orleans, U.S.A., pp. 475–478 (1987).

[12] Ohnishi A. et al.: "Simultaneous measurement of solar absorptance and total hemispherical emittance", SAE 1988 TRANSACTIONS Journal of Aerospace, pp. 1382–1387 (1988).

[13] Ohnishi A., Nakamura Y., Kawada Y., and Hayashi T.: "Simultaneous measurement of solar absorptance and total hemispherical emittance on a scientific satellite AKEBONO", 4th European Symposium on Space Environmental Control Systems, Florence, Italy, esa 324, pp. 561–564 (Oct. 1991).

[14] Yamaguchi M. and Ando K.: "Mechanism for radiation resistance of InP solar cells", J. Appl. Phys., 63, 11, pp. 5555–5562 (1988).

[15] Weinberg I., Swartz C. K., Hart R. E., and Yamaguchi M.: "Radiation damage in proton irradiated indium phosphide solar cells", Proc. 5th European Symposium Photovoltaic Generators in Space, The Hague/Scheveningen, The Netherlands, esa SP-267, pp. 415–420 (1986).

[16] Loo R., Knechtli R. C., and Kamath G. S.: "Enhanced annealing of GaAs solar cell radiation damage", Proc. 15th IEEE Photovoltaic Specialists Conference, New York, U.S.A., pp. 33–37 (1981).

[17] Ando K. and Yamaguchi M.: "Radiation resistance of InP solar cells under light illumination", Appl. Phys. Lett., 47, 8, pp. 846–847 (1985).

[18] Yamaguchi M., Ando K., and Uemura C.: "Carrier concentration effects on radiation damage in InP", J. Appl. Phys., 55, 8, pp. 3160–3162 (1984).

[19] Yamaguchi M. and Nagai O.: "Effects of impurities on gamma-irradiated silicon crystal examined by photovoltaic effect of P-N junction diode", Jpn. J. Appl. Phys., 11, 7, pp. 1016–1023 (1972).

[20] Yamaguchi M. and Uemura C.: "Changes in the electrical properties of GaAs due to electron irradiation", J. Appl. Phys., 57, 2, pp. 604–606 (1985).

[21] The Institute of Electrical Engineers of Japan: "Solar cell handbook", Corona Publishing Co., Ltd., p. 122 (1985) (in Japanese).

[22] Uesugi K., Kawaguchi J., Shuto M., Ishii N., Kamimura M., Ishii S., Kimura M., and Tanaka K.: "Trajectory design and control of a multiple lunar swingby orbit for MUSES-A", Proc. 17th International Symposium on Space Technology and Science, Tokyo, pp. 647–652 (1990).

[23] Tada H. Y., Carter Jr. J. R., Anspaugh B. E., and Downing R. G.: "Solar cell radiation handbook", Third Edition, JPL Publication 82–69 (1982).

[24] Yamaguchi M., Hayashi T., Ushirokawa A., Takahashi K., Takamoto T., Okazaki H., Ohmori M., Ikegami S., and Arai H.: "Analysis of space fiight data of InP solar cells in EXOS-D orbit", Proc. 22nd IEEE Photovoltaic Specialists Conference, Las Vegas, U.S.A., pp. 1576–1581 (1991).

[25] Takahashi K., Kohbata M., Ohnishi A., Hayashi T., Ushirokawa A., Yamaguchi M., Ikegami S., Hashimoto K., Arai H., Orii T., Takamoto T., Okazaki H., Takamura H., Ura M., and Ohmori M.: "InP solar cells for scientific satellite applications", Proc. European Space Power Conference, Florence, Italy, esa SP-320, pp. 501–506 (1991).